Published in final edited form as:

*Cancer Res*. 2023 December 15; 83(24): 4142–4160. doi:10.1158/0008-5472.CAN-23-0883.

# Prostate cancer progression relies on the mitotic kinase citron kinase

**Chitra Rawat**[1,*], **Salma Ben-Salem**[1,*], **Nidhi Singh**[1], **Gaurav Chauhan**[1], **Anja Rabljenovic**[1], **Vishwa Vaghela**[1], **Varadha Balaji Venkadakrishnan**[1,a], **Jonathan D. Macdonald**[3,b], **Ujjwal R. Dahiya**[1], **Yara Ghanem**[1], **Salam Bachour**[4,c], **Yixue Su**[1], **Adam D. DePriest**[5,d], **Sanghee Lee**[6,e], **Michelle Muldong**[6,f], **Hyun-Tae Kim**[6,7], **Sangeeta Kumari**[1,g], **Malyn May Valenzuela**[1,h], **Dingxiao Zhang**[8,9], **Qiang Hu**[8], **Eduardo Cortes Gomez**[8], **Scott M. Dehm**[10], **Amina Zoubeidi**[11], **Christina A.M. Jamieson**[6], **Marlo Nicolas**[12], **Jesse McKenney**[12], **Belinda Willard**[13], **Eric A. Klein**[14], **Cristina Magi-Galluzzi**[12,i], **Shaun R. Stauffer**[3], **Song Liu**[$,8], **Hannelore V. Heemers**[$,1]

[1]Department of Cancer Biology, Cleveland Clinic, Cleveland, OH 44195

[3]Center for Therapeutics Discovery, Cleveland Clinic, Cleveland, OH 44195

[4]Cleveland Clinic Lerner College of Medicine, Cleveland Clinic, Cleveland, OH 44195

[5]Department of Cancer Genetics, Roswell Park Comprehensive Cancer Center, Buffalo, NY 14623

[6]Department of Urology, UC San Diego, La Jolla, CA92093

[7]Department of Urology,School of Medicine, Kyungpook National University, Daegu, Republic of Korea

[8]Department of Biostatistics and Bioinformatics, Roswell Park Comprehensive Cancer Center, Buffalo, NY 14623

[9]School of Biomedical Sciences, Hunan University, Changsa 410082, China

**To whom correspondence should be addressed**: Dr. Hannelore Heemers, Cleveland Clinic, Department of Cancer Biology, Lerner Research Institute, NB-40, 9500 Euclid Avenue, Cleveland, OH 44195 Phone: 216-4457357, email: heemerh@ccf.org.

[a]Current affiliations:
Dana Farber Cancer Institute
[b]Schrodinger New York
[c]Brigham and Women's Hospital
[d]Buffalo State University
[e]Certis Oncology
[f]Icosavax
[g]Emory University
[h]Advent Health
[i]University of Alabama at Birmingham
[*]equal contributions
[$]equal contributions

**Author contributions:** CR, SBS, NS, JDM, QH, EC, CAMJ, JW, SRS, SL, CMG and HVH conceived and designed analyses. CR, SBS, NS, VBV, GC, CR, AR, NS, UD, YG, VV, SB, YS, ADD, SL, MM, H-TK, SK, MMV, MN and BW collected data. SMD, AZ, CMG, BW and EK contributed data or analysis tools. CR, NS, SBS, CR, NS, VBV, DZ, QH, EC, JW, SL, MN, CMG and HVH performed analyses. CAMJ, JM, SRS, SL and HVH supervised analyses. HVH, VV, CR and SBS wrote the paper. All authors reviewed and approved the submitted manuscript.

**Conflict of interest statement**: Shaun R. Stauffer, Hannelore V. Heemers, Jonathan D. MacDonald and Salma Ben-Salem are inventors on US patent application 63/170,898 "Citron kinase inhibitors". The other authors have declared that no conflict of interest exists.

[10]Masonic Cancer Center and Departments of Laboratory Medicine and Pathology and Urology, University of Minnesota, Minneapolis, MN 55455

[11]Vancouver Prostate Centre and Department of Urologic Sciences, University of British Columbia, Canada

[12]Department of Anatomic Pathology, Cleveland Clinic, Cleveland, OH 44195

[13]Department of Proteomics Core Facility, Cleveland Clinic, Cleveland, OH 44195

[14]Department of Urology, Cleveland Clinic, Cleveland, OH 44195

## Abstract

Prostate cancer (PCa) remains the second leading cause of cancer death in men in Western cultures. Deeper understanding of the mechanisms by which PCa cells divide to support tumor growth could help devise strategies to overcome treatment resistance and improve survival. Here, we identified that the mitotic AGC family protein kinase citron kinase (CIT) is a pivotal regulator of PCa growth which mediates PCa cell interphase progression. Increased CIT expression correlated with PCa growth induction and aggressive PCa progression, and CIT was overexpressed in PCa compared to benign prostate tissue. CIT overexpression was controlled by an E2F2-Skp2-p27 signaling axis and conferred resistance to androgen targeted treatment strategies. The effects of CIT relied entirely on its kinase activity. Conversely, CIT silencing inhibited growth of cell lines and xenografts representing different stages of PCa progression and treatment resistance but did not affect benign epithelial prostate cells or non-prostatic normal cells, indicating a potential therapeutic window for CIT inhibition. CIT kinase activity was identified as druggable and was potently inhibited by the multi-kinase inhibitor OTS-167, which decreased proliferation of treatment-resistant PCa cells and patient-derived organoids. Isolation of the in vivo CIT substrates identified proteins involved in diverse cellular functions ranging from proliferation to alternative splicing events that are enriched in treatment-resistant PCa. These findings provide insights into regulation of aggressive PCa cell behavior by CIT and identify CIT as a functionally diverse and druggable driver of PCa progression.

### Keywords

androgen deprivation therapy; treatment resistance; oncogenic driver; phosphorylation; cell proliferation

## Introduction

In 2023, more than 34,000 American men will die from prostate cancer (CaP) because metastatic disease becomes resistant to administered treatments (1). Androgen receptor (AR), a major driver of CaP progression, remains the main target for such treatments. First-line androgen deprivation therapy (ADT) and addition of novel ADTs including enzalutamide and abiraterone induces remissions but eventually fails with the majority of recurrent disease consisting of castration-resistant CaP (CRPC) that still relies on AR for growth (2) and a minority of AR-indifferent or AR-negative neuroendocrine CaP (NEPC)

(3). Alternative treatments include chemo- or radio-therapy (4), which yield brief remissions but do not cure CaP.

The molecular determinants that control CaP progression remain incompletely understood (5). Here, we explored the mitotic kinase citron kinase (CIT) as an unrecognized regulator of CaP cell proliferation and novel functionally diverse and druggable target. Because it binds activated Rho GTPases, CIT was originally thought to be a Rho effector (6). Today, it is clear that CIT primarily acts as a key regulator of cytokinesis or cell division (7, 8). In our previous studies examining CaP signal transduction from RhoA to the transcription factor Serum Response Factor, CIT also did not serve as mediator (9). CIT is now well-recognized to control spindle formation during metaphase and midbody formation during late telophase, yet its involvement in DNA damage repair, virion production and exocytosis suggest it also exerts functions during interphase (7).

CIT is an AGC family serine/threonine protein kinase that is one of two major isoforms encoded by the CIT gene (6, 10, 11). The other isoform, citron-N, differs from CIT only by the absence of a kinase domain. CIT is ubiquitously expressed in proliferating cells whereas citron-N is found only in the central nervous system (CNS) (6, 10, 12, 13). Despite CIT's role in cytokinesis, mammals with germline loss of CIT or loss-of-function CIT mutations are viable. Such alterations mainly delay CNS development (7, 8), suggesting that therapeutic interference with CIT in adult men in whom CNS development is complete may not cause severe side effects.

We found that CIT controls proliferation of CaP but not benign cells. CIT overexpression during CaP progression associated with pluripotency and mediated CaP aggressiveness and growth under treatment resistance. CIT relied on its kinase function for its effects on CaP and was druggable with CIT inhibition decreasing growth of treatment-naïve and resistant CaP. The CIT-dependent CaP phosphoproteome covered roles in cell proliferation, but also in other processes such as alternative splicing, a hallmark of CaP aggressiveness (14).

Our studies thus provide novel insights into the molecular mechanisms in control of CaP cell proliferation, support a rationale for CIT as a novel therapeutic target, and isolate CIT's kinase activity as a determinant of CaP progression.

## Materials and methods

### Reagents

R1881 (R0908), dihydrotestosterone (A8380), dimethyl sulfoxide (DMSO, D2438), doxycycline (D3072), palbociclib/PD-0332991 (PZ0199), roscovitine (R7772), aphidicolin (178273), hydroxyurea (H8627), nocodozole (M1404), biotin (B4501), and MG-132 (474788) were obtained from Sigma-Aldrich. Polybrene (sc134220) was from Santa Cruz Biotechnologies. Trypan blue (15250061), zeocin (R25001) and Halt protease inhibitor cocktail (100x, 78429) were from Thermo-Fischer Scientific, blasticidin (A11139–03), fetal bovine serum (FBS, 10437028), DynaBeads protein G (10004D) and Dynabeads M-280 streptavidin (11205D) from Life Technologies, Tet System Approved FBS (631107) and puromycin (631305) from Clontech. Enzalutamide (S1250), tofacitinib (S2789), Y-39983

(S7935), apitolisib (S2696), dacomitinib (S2727) and OTS-167 (S7159) were purchased from Selleck Chemicals. siRNAs targeting CIT, AR, E2F1, E2F2, E2F3, E2F4, Skp2, p27, RB1, THRAP3 and MATR3 and non-targeting control siRNAs were obtained from ThermoScientific (M-004613–00-0005, M-003400–02-0005, M-003259–01-0005, M-003260–02-0005, M-003261–02-0005, M-003262–04-0005, M-003324–04-0005, M-003472–00-0005, M-003296–03-0005, M-019907–01-0005, M-017382–01-0005, and D-001810–10-20, respectively). Antibodies were purchased from BD (CIT/CRIK (611377, western blotting)), Santa Cruz Biotechnologies (AR (sc-7305), CIT/CRIK (sc-1848, IHC), OCT4 (sc-5279), cyclin A (sc-271682)), Abcam (Ki67 (ab15580), sodium potassium ATPase (ab76020), MATR3 (ab151714), E2F2 (ab138515), Cell Signaling (E2F1 (3742), Skp2 (2652), p27 (3686), vimentin (3932), slug (9585), β -actin (4967), pRB Ser780 (C84F6), Rb (9309), phospho-histone 3 H3 Ser10 (9701), cyclin B1 (4138), MLC2 (8505), pMLC2-S19 (3671), pMLC2-T18S19(95777), cleaved PARP (9541), PARP (9542), histone 3 (4499), ubiquitin (3933), normal rabbit IgG (2729), anti-rabbit IgG-HRP linked (7074), anti-mouse IgG Alexa Fluor 594 (8890) and anti-rabbit IgG Alexa Fluor 488 (4412)), Millipore (anti-mouse IgG (12–371), Novus (Sox2 (AF2018), THRAP3, (NB100–40848)), ThermoFisher (anti-pSer, 500–021), Fisher Scientific (anti-mouse-HRP, 45000679), Sigma-Aldrich (FLAG, F3165), and LiCoR (IRDye 800 CW Donkey anti-Goat IgG secondary antibody, 926–32214). Vectashield mounting media with DAPI was from Vector Laboratories (94010, H-1200). Kpn1 (R0142), NotI (R0189), EcoRI (R0101) and XbaI (R0145) restriction enzymes were purchased from New England BioLabs. SMARTvector 2 inducible human CIT mCMV-turboGFP shRNA (V3IHSMCG_4880171, V3IHSMCG_6330422, V3IHSMCG_10221683) lentiviral particles were purchased from Thermo-Scientific (see Supplementary Information Table 1 for sequences).

## Cell culture

LNCaP, VCaP, PC3, DU145, and RWPE1 cells were purchased from ATCC. C4–2 cells were obtained from Uro-Cor. R1-D567 cells (15) were a gift from the Scott Dehm laboratory. V16D, 49C$^{ENZR}$, 49F$^{ENZR}$, 42D$^{ENZR}$, and 42F$^{ENZR}$ cells (16) were provided by the Amina Zoubeidi laboratory. NIH-3T3 and 293T cells were obtained from the Cleveland Clinic Lerner Research Institute Cell Services core facility. Cells were cultured as before (9, 15–17) for a maximum of 10 passages and were Mycoplasma-tested using the LookOut® Mycoplasma PCR Detection Kit (Sigma-Aldrich, MP0035). Cell lines were authenticated via short tandem repeat profiling by LabCorp (NIH-3T3 and 293T) or Genetica DNA Laboratories (all other lines). For growth-stimulation, CaP cells were cultured for 2 days in steroid-depleted media and then treated with either vehicle (ethanol) or different doses of R1881 or DHT. For FBS stimulation, cells were serum-starved for 24h followed by FBS re-administration. Generation of stable cell lines is described below.

## Generation of expression plasmids

The CIT open reading frame was subcloned from a human CIT expression vector (SC303887, Origene) into the restriction sites KpnI and NotI of the pcDNA3.1+ (Life Technologies) multiple cloning site. The T-REx™ System consisting of pcDNA6/TR (V102520) and pcDNA4/TO plasmids (V102020) (Thermo-Scientific) was used to inducibly overexpress CIT. The coding sequence of CIT was subcloned into the KpnI and NotI

restriction enzyme sites in the multiple cloning sites of pcDNA4/TO vector (Invitrogen). Expression constructs encoding kinase-dead CIT-KD (K126A) were generated using the Quick Change II XL Site-Directed mutagenesis kit (Agilent, 200521). The E2F2 open reading frame (NM_004091) was subcloned from a human untagged expression vector (SC303431, Origene) into the restriction sites EcoRI and XbaI of the p3xFLAG-CMV-10 plasmid. The HA-Turbo-ID expression construct (#107171) was a kind gift from the laboratory of Dr. Kurt Runge at Cleveland Clinic. The CIT coding sequence was cloned in frame in KpnI and NotI multiple cloning sites of the 3xHA-TurboIS-pcDNA3 cloning sites. Sequence integrity of all expression constructs was verified by Sanger sequencing. Primers used for cloning and site-directed mutagenesis are listed in Supplementary Information Table 1.

## Generation of stably transfected CaP sublines

The T-Rex System was used to establish a stable LNCaP subline that allows for inducible expression of CIT. To this end, LNCaP cells were transfected with pcDNA6TR plasmid using TransFast (Promega, E2431) according to manufacturer's instructions. Two days after transfection, cells were subjected to selection using 10 μg/ml blasticidin. A polyclonal subline was generated in which expression of TR was verified using a specific antibody (TetR clone 9G9, Clontech). The LNCaP-pcDNA6TR subline was then transfected with pcDNA4/TO-CIT using Viromer transfection reagent as per manufacturer's instructions. After 2 days, polyclonal sublines with inducible CIT expression were selected for in medium supplemented with 10 μg/ml blasticidin and 1 μg/ml zeocin. Inducible expression of CIT-KD in the resulting stable cell line was verified via western blotting after 48h treatment with 1 μg/mL of doxycycline. LNCaP and R1-D567 sublines that allowed for inducible expression of shRNA targeting CIT were generated by transducing CaP cells with CIT-specific SMART vector 2 System lentiviral particles according to the manufacturer's instructions. Three individual SMARTvector Inducible Human mCMV-turboGFP shRNAs were used to generate stable cell lines (Supplementary Information Table 1). Cells were seeded onto 96-well plates at a density of 5,000 cells/well. The next day, cells were transduced with serial dilutions of three different retroviral particles in regular media with polybrene 5μg/ml for 12h. Polyclonal sublines that stably expressed CIT shRNA were selected using 1 μg/mL of puromycin. Efficiency of shRNA-mediated knock down of CIT was verified via western blotting following doxycycline treatments of cells compared to vehicle (DMSO).

## siRNA and plasmid transfections

siRNAs were transfected into CaP cells using Lipofectamine 2000 (Invitrogen) or Oligofectamin (Invitrogen) as before (9, 16, 17). Transient plasmid transfections were done via electroporation (9, 17) or using Viromer Red (Lipocalyx, VR-01LB-01) or Fugene HD (Promega, E2311) transfection reagents following the manufacturer's protocols.

## Cell viability, cell proliferation and cell cycle analyses

Cell viability, cell proliferation examination via Ki67 immunocytochemistry, cell cycle FACS and tryphan blue exclusion assays were done as before (17).

## Cell cycle enrichment studies

LNCaP cells were seeded in FBS-supplemented medium. The next day, cells were treated with either 0.5μM PD-0332991 (early G1 phase enrichment), 5μg/mL roscovitine (late G1 phase enrichment), 2μg/mL aphidicolin (early S enrichment), 1mM hydroxyurea (late S enrichment) for 24h, or with 2μg/mL aphidicolin for 15h, followed by 2 washes with 1X PBS and treatment with 50ng/mL nocodozole for 9h (G2/M phase enrichment) (18).

## Immunohistochemistry, polyploidy and other immunostaining assays

### Analysis of CIT protein expression in clinical CaP tissues

**CIT immunohistochemistry on CaP tissue microarray (TMA):** CaP TMAs that contained 200μm cores from radical prostatectomy specimens were generated at the Cleveland Clinic under IRB approval which included the patient's written informed consent. The TMAs were composed of 149 CaP cores, of which 121 included adjacent benign prostate tissue cores. Tissues were obtained from patients who had not been treated with hormonal, chemo- or radiation therapy prior to radical prostatectomy. All specimens were inspected for tissue content and quality by a board-certified GU pathologist.

**CIT immunohistochemistry:** TMA sections, 5μm thick, were deparaffinized, rehydrated using an alcohol gradient, and subjected to antigen retrieval. IHC was performed using a goat polyclonal CIT/CRIK antibody (sc-1848, Santa Cruz Biotechnology Inc.) diluted 1:25 and detected using the ChromoMap DAB IHC Kit (Ventana Medical Systems Inc.). Hematoxylin II staining (Ventana) was used for background staining. Images were scored for CIT staining using a technique we described before (17); one reviewer who was blinded scored each TMA. For each core, CIT staining intensity was scored as 0, 1, 2, or 3, which corresponded to absent, weak, moderate, or strong staining, respectively.

### Polyploidy and other immunostaining assays

CaP cells seeded on coverslips were fixed using ice-cold methanol, blocked and incubated with an antibody targeting Na+/K+ ATPase (1:500 dilution) for 1h at room temperature. Cells were stained with Alexa Fluor 488 (Cell Signaling) secondary antibody. Coverslips were mounted and nuclei were counterstained with DAPI as before (17). Images were taken using an inverted EVOS FL imager (ThermoFisher Scientific) at 20X magnification. Images of single sections in the z-plane were merged, contrast-enhanced and the number of multinucleated cells was quantified using Image J (v1.43).

## Western Blotting

Western blotting was performed using the Novex system (Thermo Fisher Scientific) as before (9, 17) or using a LICOR Odyssey CLx detection instrument and Image studio software version 5.2. Quantification of immunoreactive signals was performed using Image Studio software (LI-COR) Ver 3.1. The value of an immunoreactive signal was normalized using the value of the matching input or loading control sample.

### RNA isolation and qRT-PCR

RNA extraction, cDNA preparation and qRT-PCR were performed as we have done previously (17). Primers are listed in Supplementary Information Table 1.

### RNA-Seq studies

LNCaP cells were transfected with siRNA against CIT, E2F1 or E2F2 or control siRNA as before (9, 17). At 48h post transfection, cells were treated with 0.1nM R1881 or vehicle (ethanol). Biological triplicates were performed for each treatment group. Cells were harvested 48h later, and RNA was isolated and column purified using RNAeasy columns (Qiagen). RNA-Seq for CIT-depleted and matching control samples was done at the Genomics Core facility at the Cleveland Clinic's Lerner Research Institute. In brief, 1μg total RNA was quantified using a QuBit Fluorometer 3.0 (Invitrogen) and checked for integrity using a 2100 Bioanalyzer (Agilent) according to manufacturer's instructions. Sequencing libraries were constructed using the TruSeq Stranded Total RNA Library Prep Kit (Illumina), and sequencing adaptors were ligated by PCR. The constructed library was assessed using a QuBit Fluorometer 3.0, 2100 Bioanalyzer, and quantitated using the KAPA Library Quantification Kit (Roche) by qPCR. Sequencing was performed with a HiSeq 2500 (Illumina) sequencing platform using paired-end 100 bp chemistry following the manufacturer's recommended protocol. RNA-Seq for E2F1-depleted, E2F2-depleted and control siRNA-transfected samples was performed at Roswell Park Comprehensive Cancer Center as previously described (9). RNA-Seq data were deposited in GEO under accession numbers GSE123970 and GSE172094.

The DESeq2 package was used to identify differentially expressed genes from RNA-Seq data. CIT growth-repressed and CIT growth-induced genes were defined as in Supplementary Figure 1. In addition, genes that showed at least 2-fold change at their basal expression (vehicle treatments) after CIT depletion compared to siRNA control samples were isolated as described in Supplementary Figure 1. CIT-dependent gene signatures are listed in Supplementary Information Table 2. Pathway enrichment analysis was performed from the CIT growth-repressed and growth-induced gene signatures and CIT-dependent basal gene sets (up-regulated, down-regulated), utilizing hallmark gene sets and oncogenic gene sets from the Molecular Signature Database (MSigDB). The association of these gene signatures with clinical CaP progression was verified via GSEA analyses on gene expression profiles from CaP patient specimens, with the recommended threshold of false discovery rate (FDR) of 0.25.

Analysis of CIT-dependent alternative splicing events was done using rMATS tools as described before (14). Five types of alternative splicing events based on the GENCODE gene annotation were evaluated, including skipped exon (SE), alternative 5′ splice site (A5SS), alternative 3′ splice site (A3SS), mutually exclusive exons (MXE) and retained intron (RI). The events with an inclusion-level difference of at least 10%, and FDR <0.1 were determined as differential alternative splicing events.

Exon usage changes among alternatively spliced isoforms across different samples and experimental conditions were visualized and compared using Sashimi plots (19). Specific

primer sets used to validate the identified changes among CIT-dependent alternatively spliced transcripts are described in Supplementary Information Table 1. PCR was carried out in triplicates using PrimeStar GXL DNA Polymerase (Takara-Clontech) according to the manufacturer's instructions. PCR amplicons were resolved on 4%–5% agarose gels; GAPDH was evaluated as a control to assess variation between replicates and treatments.

### The Prostate Cancer Transcriptome Atlas (PCTA) analyses

The PCTA web tool was used to mine available PCTA and TCGA CaP gene expression data sets by CaP subtype information based on Gleason score and metastasis status (20). CIT-dependent gene signatures (Supplementary Information Table 2) were analyzed in the PCTA correlation view analysis function against publically available signatures relevant to mitosis, AR activation, castration resistance and stemness. Specifically, a CIT-controlled signature was compared to relevant gene sets derived from GSEA (21): GeneSet mitosis (mitosis), hallmark mitotic spindle, hallmark androgen response, Bhattacharya_embryonic_stem cell gene set (embryonic stem cells) and the Wong_adult_tissue_stem_module gene set (adult stem cells). Other signatures used for correlation view comparisons were derived from literature: the Hieronymus AR activity signature (22), a 452-AR-target gene signature derived by our group (22), 16 AR target genes that represent rewired AR action in CRPC and predict CRPC recurrent disease ("CRPC-16AR") (23), and the META16 signature of 16 genes that are prognostic for time to metastasis and response to AR-targeting therapies (24). The correlation coefficient and p value derived from each of the PCTA analyses were recorded and represented graphically using R version 4.0.0 with plots generated using the ggplot2 (v3.3.3) software.

### Co-immunoprecipitation

CoIPs were done for endogenously expressed proteins. Cell pellets were lysed in lysis buffer (20 mM Tris (pH 8.0), 150 mM NaCl, 5 mM MgCl2, 0.5% NP40 and 1X EDTA-free protease inhibitor cocktail (Roche), phosphatase inhibitor (Active Motif) for 1h at 4°C. Protein concentration was estimated using a Bradford assay (Promega). Protein lysates (2mg) were incubated with 6 μg primary antibodies or non-specific IgG overnight at 4°C. DynaBeads were equilibrated for lysis buffer for 1h at 4°C. The next day, immune-complexes were precipitated using Dynabeads (protein G) at 4°C for 3h. Beads were washed 5 times with washing buffer (20 mM Tris, (pH 8.0), 150 mM NaCl, 0.25% NP40, 1X EDTA-free protease inhibitor cocktail (Roche) and 1x phosphatase inhibitor buffer (Active Motif)). Samples were eluted with 2x SDS-PAGE NOVEX sample buffer and 2x reducing agent (ThermoFisher) and heated at 70°C for 10 min.

### CIT IP-MS with phosphoenrichment

Cell pellets were collected and harvested for endogenous CIT IP as described. The next day, immune-complexes were precipitated and washed following our Co-IP protocol and stored in washing buffer at 4°C.

Immunoprecipitates were subjected to on-bead tryptic digestion (25). Briefly, trypsin (10 μl, 10 ng/μl) in 100 mM ammonium bicarbonate was added to wash beads, and samples vortexed for 15 sec every 2–3 min for 15 min to ensure uniform suspension of beads.

Digestion was continued overnight at 37°C. A second 10-μl trypsin aliquot was added for 4h at 37°C. The supernatant was collected on a magnetic rack and diluted with formic acid (5% final concentration). The digests were cleaned using PepClean C-18 spin columns (ThermoScientific) according to manufacturer's instructions, the samples dried in a SpeedVac, and reconstituted in 1% acetic acid.

One aliquot (25% of total protein lysate) of each digest was analyzed directly by LC-MS and the second aliquot (75% of total protein lysate) was subjected to phosphopeptide enrichment. For phosphopeptide enrichment, digests were dried in a Speedvac then reconstituted in 50 μl binding buffer (1 M glycolic acid in 80% acetonitrile, 5% trifluoroacetic acid). Phosphopeptide enrichment was performed using two different methods, TiO2 Mag Sepharose (GE Healthcare Piscataway, NJ) magnetic beads and porous zirconium dioxide TopTip (GlyGen, Anoka MN) pipette tips. Peptide binding, washing, and elution was performed according to manufacturer's instructions. The eluted peptides were evaporated to <10μl and reconstituted in 15μl of 1% acetic acid.

The LC-MS system was a Fusion Lumos Tribrid MS (ThermoScientific) equipped with a Dionex Ultimate 3000 nano UHPLC system and a Dionex (25 cm × 75 μm id) Acclaim Pepmap C18, 2-μm, 100-Å reversed-phase capillary chromatography column. Peptide digests (5-μl) were injected and eluted with an acetonitrile/0.1% formic acid gradient at a flow rate of 0.3 μl/min. Experiments were analyzed using a data-dependent acquisition method that utilizes MS1 scans to identify peptide molecular weights and collision-induced dissociation-based MS2 scans to identify peptide sequences. For the proteomic analysis, the data were analyzed using MaxQuant V1.5.2.8 with the search engine Andromeda which is integrated into MaxQuant software, and the parameters used were the default settings for an Orbitrap instrument. To search the MS/MS spectra, we used the Uniprot human protein database, which contains 20,429 entries with an automatically generated decoy database (reversed sequences). We searched for fully tryptic peptides with a maximum of two missed cleavages. Oxidation of methionine and acetylation of the protein N-terminus were set as dynamic modifications. The precursor mass tolerance for these searches was set to 10 ppm and the fragment ion mass tolerance was set to 0.5 Da. The search included the common contaminant database available in MaxQuant and these proteins were excluded in the data analysis. The FDR was set to 1% for both peptide and protein with a minimum length of 7 amino acids, two unique or razor peptides were required for positive identification. The "match between runs" feature of MaxQuant was used to transfer identifications to other LC-MS/MS runs based on their masses and retention time (maximum deviation 0.7 min) and this feature was also used in quantification experiments. Quantification was performed with the label-free quantitation method available in the MaxQuant program (26).

For the phosphoproteomic analysis, collected data were searched using the same parameters as the above with the addition of phosphorylation as a variable modification at S, T, and Y residues and these searches were performed using Proteome Discoverer 2.4 (ThermoScientific). Quantitation was performed by aligning chromatograms, normalizing to total peptide amount, and calculating the normalized LFQ intensities for each peptide. Phosphopeptides that occurred in the CIT IP only (not in the IgG IP) or for which values in the CIT IP were at least 2-fold greater than those in the IgG IP were withheld for analysis.

The peptide peak intensities were used for these comparisons. Potential CIT-interacting partners were analyzed for GO gene sets, hallmark gene sets, and curated gene sets (MSigDB), with the recommended threshold FDR of 0.25.

### Biotin-based proximity ligation assays coupled with MS

For protein-proximity labelling (27), 10 million LNCaP cells were electroporated using 5ug TurboID constructs (3xHA-TurboID-CIT, 3xHA-TurboID-CIT-kinase dead, or empty vector). Electroporated cells were cultured in DMEM media. After 48h, fresh DMEM media was added, and cells were treated with 50μM biotin or DMSO (vehicle) for 18h. Cell pellets were harvested, lysed and protein concentration was quantified by Bradford assay. Cell lysates were incubated with equilibrated strep-conjugated Dynabeads (50μl/sample) overnight at 4°C. The next day, immune-complexes were precipitated, washed and stored as described above. Immunoprecipitate digestions, MS and MS data analysis were done as described above.

Phosphopeptides for which values were ≥3-fold above those observed in the no-biotin empty TurboID vector transfected condition in the wild-type CIT condition, increased ≥2 fold (for most entries ≥10-fold) above vehicle with biotin treatment in the wild-type CIT Turbo vector condition, and for which biotin-induction was reduced ≥40% in the CIT-KD version compared to the wild-type CIT transfection, and were lower than empty vector control were withheld for analysis. The peptide peak intensities were used for these comparisons. MSigDB was done as above with the recommended FDR threshold of 0.25.

### Subcutaneous CaP xenografting

Animal studies were conducted after approval by the Cleveland Clinic's IACUC. $1\times10^7$ LNCaP or R1-D567 cells that expressed one of two doxycycline-inducible shRNAs targeting CIT (shRNA#2 or #3, respectively) were injected subcutaneously in matrigel (Fisher Scientific, 356234, 1/1 v/v) in the flank of 6- to 8-week-old male outbred homozygous nude (*Foxn1*$^{nu}$/*Foxn1*$^{nu}$) mice (strain 007850) from the Jackson Laboratory. Once the tumor volume reached 100 $mm^3$, mice were randomly assigned to treatment groups and administered 200μg/ml doxycycline in drinking water or vehicle (DMSO) for 28 days. Treatment was repeated every other day by replacing drinking water with fresh water supplemented with doxyxcycline. Tumor volume was calculated using the formula 0.52*tumor length*tumor width$^2$ based on caliper measurements done every other day.

For the tumor development experiments using the LNCaP cell line that allows for inducible CIT expression, mice were castrated and 2 weeks later, $1\times10^7$ cells were injected subcutaneously in matrigel the flank of BALBc nu/nu mice as above. Immediately following injection of cells, mice were randomized to treatment with doxycyclin (20 μg/ml in drinking water) or vehicle (DMSO). Treatment was repeated every other day by replacing drinking water with fresh water supplemented with doxyxcycline. Tumors measured using calipers every other day, for 140 days, as above.

### 3D organoid cultures from patient-derived xenografts

The protocol to establish organoids from the PCSD1 PDX was adapted from Drost *et al.* (28). PCSD1 cells were resuspended in growth factor-reduced Matrigel (BD Biosciences) at a concentration of 25,000 cells per 20 μL of Matrigel. Aliquots of the cell suspension were domed on cell culture plates according to the seeding concentration as previously described. To prevent cells from adhering to the bottom of the plate, tissue culture plates were inverted for 15 minutes prior to being placed in the $CO_2$ incubator (5% $CO_2$, 37°C). Once the domes solidified, the appropriate volume of medium was added to each well. Media formulations were modified with the addition of 10% FBS. Medium was changed every 3 to 4 days and fresh medium was made every week. After 7 days, cultures were grown in medium without the Rho-kinase inhibitor Y-27632.

After 2 weeks of culturing, OTS-167 was dissolved in DMSO and added to the culture medium at a final concentration of 50 μM. The vehicle control conditions were 0.1% (v/v) DMSO in culture medium. Each experimental condition (DMSO, OTS-167) was set up in quadruplicate. The epithelial cyst lumen diameter, cyst counts, spheroid area, and spheroid counts were observed using a Keyence BZ-X710 microscope (Keyence Corporation). Lumen diameter was measured with an adjustable scale bar using the Keyence microscope software. Spheroid area was measured using the Keyence Hybrid Cell Counter at 4X magnification by outlining spheroid clusters that were at least 50 μm in size with the Free Draw Tool by 3 independent observers. Cysts with diameter greater than 50μm and spheroids with area greater than 2500$\mu m^2$ were analyzed.

### In vitro kinase assays

Efficiency of OTS-167, Y39983, tofacitinb, apitolisib, and dacomitinib to inhibit CIT activity was determined using CIT/CRIK Human AGC Kinase Enzymatic LANCE Assay in vitro kinase assays (Eurofins 2628). The $IC_{50}$ of each kinase inhibitor was calculated using GraphPad.

### Statistics

Except for RNA-Seq, organoid and xenograft studies, at least 2 independent experiments were performed. Data are presented as the mean ± standard error of the mean. To compare the difference between two groups, student's t-test was used (SigmaPlot version 14.5). Differences among groups in xenograft studies were evaluated using 2-way ANOVA tests (SigmaPlot version 14.5). To evaluate the statistical significance of overlap between two sets of genes, two-tailed Chi-squared test was used. All statistical tests are 2-tailed unless otherwise specified. Significance was set at <0.05.

### Data availability statement

RNA-Seq data generated in this study were deposited in GEO under accession numbers GSE123970 and GSE172094. The gene expression data comparing CRPC and treatment-naive CaP analyzed in this study were obtained from the GEO database at GSE32269 (https://www.ncbi.nlm.nih.gov/geo/query/acc.cgi?acc=gse32269). GSEA data analyzed in this study were obtained from https://www.gseamsigdb.org/gsea/. TCGA and PCTA datasets

analyzed in this study were obtained from http://www.thepcta.org. All other raw data are available upon request from the corresponding author.

## Results

### CIT is induced by growth stimuli and controls CaP cell proliferation

When AR-positive LNCaP cells were treated with low doses (<1nM) of the synthetic androgen R1881, which induce CaP cell proliferation (29–31), CIT protein expression markedly increased. Only the larger CIT isoform (230 kDa) harboring the kinase function was detected (Figure 1A). CIT protein induction by growth-inducing R1881 doses was validated in AR-positive VCaP cells (Figure 1B) and by using low doses of the natural androgen dihydrotestosterone (Figure 1C). Low dose androgen stimulation of AR-negative PC3 cells did not induce CIT protein and in VCaP and LNCaP cells impacted CIT mRNA levels to a much lesser degree (Supplementary Figure 2 A,B). Another growth-inducing condition, re-administration of FBS after 24h serum starvation, also stimulated CIT expression (Figure 1D). However, conditions that restrict proliferation of AR-positive CaP cells, such as higher doses of androgens (>1nM), short-term treatment with enzalutamide or silencing of AR, decreased CIT expression (Figure 1A–B, Supplementary Figure 2C). These findings indicate that CIT protein levels increase under conditions that support CaP growth (FBS restoration, low dose androgens) but not when CaP growth is restricted (higher androgen doses). CIT silencing significantly decreased cell viability induced by 0.1nM R1881 or re-administration of FBS after serum starvation, indicating a causal role for CIT in control of CaP cell proliferation (Figure 1E–F, Supplementary Figure 2D). siRNA-mediated silencing of CIT decreased viability of LNCaP and VCaP cells also under regular culturing conditions, but did not affect the benign prostate epithelial cell line RWPE1, non-prostate normal NIH-3T3 or 293T cells (Figure 1G,H), suggesting a CaP-specific role for CIT. Loss of CIT reduced the number of Ki67-positive LNCaP and VCaP cells (Supplementary Figure 2E), confirming effects were due to decreased cell proliferation. FACS analyses verified delayed cell cycle progression (Figure 1I) in CIT-depleted cells: 72h and 96h post-transfection, the percentage of cells in G1 phase increased while that in S and G2/M phase decreased. At 120h, the cell number in G2/M phase started to increase relative to control cells. CIT knockdown was maintained at each time, suggesting a role at late G1 or early S for CIT. Enriching LNCaP cells in early G1, late G1, early S, late S or G2/M, we noted CIT levels were highest in cells enriched in G2/M phase, readily detectable already in early and late S phase while lower in early and late G1 phase (Figure 1J). These findings indicated a role for CIT in CaP cell interphase. Western blot analyses for markers of critical cell cycle progression steps confirmed intended phase enrichments, as did FACS analyses (Figure 1J, Supplementary Figure 2F,G). Consistent with the possibility for a role for CIT in G1/S transition or S phase, 72, 96, 120 and 144h after CIT silencing, aphidicolin treatment failed to enrich cells in early S phase (Figure 1K). That effects on cell cycle were accompanied by failure of cytokinesis was evident by increased numbers of multinucleated cells upon CIT silencing (Figure 1L). Results obtained with siRNA were validated using 3 independent doxycycline-inducible shRNAs targeting CIT in LNCaP cells (Supplementary Figure 2H). In xenograft studies using one of these LNCaP sublines, doxycycline-induced loss of CIT

significantly delayed xenograft growth and decreased CaP volume (Figure 1M), verifying a role for CIT in the growth of established CaP in vivo.

## CIT is overexpressed in CaP and correlates with aggressive CaP features

To assess clinical relevance, we quantitated CIT expression in CaP tissue microarrays containing 149 localized treatment-naïve CaP cores and, for 121 CaPs, matching benign prostate tissue cores. Representative IHC staining and specificity of the CIT antibody are shown in Supplementary Figure 3A and B. Of the 149 CaP cores, 136 were positive for CIT compared to 105 benign prostate cores, and more CaP cores showed stronger CIT expression than benign tissue (Figure 2A). Overall, CIT expression was higher in CaP (average score/core=1.449) compared to adjacent non-neoplastic prostate tissues (average score/core=1.099) (Figure 2B). CIT expression increased with higher Gleason scores (Figure 2C), consistent with a recent report (32). Gene Set Enrichment Analysis (GSEA) on gene sets that depend on CIT for growth-regulation or basal expression levels (obtained via RNA-Seq, Supplementary Information Table 2, Supplementary Figure 1) showed that genes that rely on CIT to maintain basal expression (downregulated after CIT loss) were significantly positively enriched in CRPC compared to localized untreated CaP, confirming the relevance of CIT to lethal CaP progression (Figure 2D, and Supplementary Figure 3C). No enrichment of CIT growth-dependent gene signatures was observed between localized and metastatic CaP, indicating their expression is maintained in CRPC, which contrasts with decreased AR target gene expression in CRPC (17, 33, 34). Sizes of each CIT-dependent gene set, selection criteria used to isolate them, and qRT-PCR validation are shown in Supplementary Figure 1. MSigDB analyses on CIT-dependent signatures confirmed roles in cell proliferation (G2/M checkpoint, E2F targets) but pointed also to functions in, for instance, EMT and mRNA processing (EIF4GI) (Supplementary Information Table 3). To verify the translational relevance of CIT action in clinical CaP, we analyzed CIT-dependent basal gene sets against several signatures representative of mitosis, AR action, castration resistance and stemness by using the Prostate Cancer Transcriptome Atlas (PCTA) webtool. PCTA calculates correlation coefficients between gene expression signatures in curated PCTA gene expression datasets and TGCA datasets. Correlation patterns were similar between TCGA and PCTA datasets, with stronger correlation coefficients observed in TCGA data. For those genes whose expression decreased upon CIT loss (thus genes that depend on CIT), positive relations were seen for signatures relevant to mitosis, metastatic CaP progression and (embryonic) stemness. Strong positive correlations were found between gene sets upregulated after CIT loss and signatures reflecting AR activation (Figure 2E). These findings suggest CIT action is linked to mitosis, metastasis and stemness in clinical CaP (most strongly in CRPC) but inversely so with AR activation, and support CIT's association with aggressive CaP progression and treatment resistance.

## CIT overexpression drives CaP growth

To verify the relevance of increased CIT expression in CaP development, progression and treatment resistance, we performed CIT overexpression studies. CIT overexpression decreased the percentage of cells in G1 phase whereas the numbers in S and G2/M increased, suggesting increases in CIT stimulate cell cycle progression (Figure 3A). These effects were not found following overexpression of a kinase-dead version of CIT (CIT-KD,

K126A, (6)), implicating CIT's kinase activity in cell proliferation. Stimulatory effects by CIT overexpression were seen also under conditions that normally restrict CaP cell proliferation such as androgen deprivation (Figure 3B), loss of AR (Figure 3C), or high doses of R1881 (Figure 3D), indicating CIT overexpression drives treatment resistance in CaP. To verify these findings in vivo, we engineered an LNCaP cell line to overexpress CIT in a doxycycline-dependent manner and confirmed that doxycycline treatment induced CIT expression and cell viability in these cells but not parental LNCaP cells. Induction of CIT-KD reduced cell viability (Figure 3E). We then grafted LNCaP cells that allow for doxycycline-inducible CIT overexpression in castrated mice, which does not support growth of parental LNCaP xenografts. None of the vehicle-treated animals developed CaP and all lived for the duration of this study (140 days). However, 5 mice from the doxycycline-treated group developed measurable CaPs and/or cachexia characteristic of advanced cancer, died or had to be euthanized before the end of the study (between day 78 and day 108) (Figure 3E). Three of these animals showed overt xenograft formation at the injection site, and presence of CaP was confirmed histologically (Figure 3F). The two other animals showed transient minor CaP growth that regressed, yet they developed subsequent cachexia. These findings suggested CIT activity is associated with tumor initiation. Dose-dependent CIT overexpression in benign epithelial RWPE1 cells also increased the number of Ki67-positive cells (Figure 3G) and induced expression of pluripotency markers (Oct4 and Sox2) and EMT markers (vimentin and Slug). Similar effects were seen in the LNCaP CaP cell line (Supplementary Figure 4A,B). These results indicated that increased CIT expression overcomes growth restriction and drives CaP progression.

## CIT expression is controlled by a novel E2F2-Skp2-p27 CaP signaling axis

We then examined the molecular mechanism(s) that control CIT expression in CaP. Time course experiments in LNCaP and VCaP cells treated with 0.1nM or 1nM R1881 or vehicle revealed that low doses of androgens (0.1nM) stimulated CIT protein expression by 24h (Figure 4A). However, at 24h post-treatment, CIT mRNA expression was not significantly altered, suggesting induction of CIT occurs post-transcriptionally (Figure 4B). Treatment with MG132 following 0.1nM R1881 or vehicle exposure increased CIT protein expression, particularly in the vehicle-treated condition (Figure 4C), indicating decreased proteasomal degradation and increased CIT stability following growth stimulation. Supporting this possibility, immunoprecipitation (IP) using a ubiquitin-specific antibody followed by immunoblotting for CIT showed increased ubiquitination levels per CIT protein levels after exposure to vehicle compared to low-dose R1881 treatment (Figure 4D). Regulators of CIT expression are largely unknown; however, one report indicated that E2F transcription factors control CIT expression in erythroblasts (35) and another that the tumor suppressor p27 binds to and inactivates CIT in mouse tissues and cells (36). E2F activity is stimulated by low doses of androgens (37) and controls expression of the E3 ligase Skp2 (38), which mediates proteosomal degradation of p27 (e.g. (39)). We similarly noted increased E2F1 and Skp2 levels and decreased p27 expression after FBS restoration (Supplementary Figure 4C). We hypothesized that activation of E2F-Skp2 signaling that leads to decreased p27 expression may control CIT expression in CaP cells. Because previous examination of E2F action in CaP cells only considered activity of E2F1 (37), we performed a small siRNA screen for E2F1, E2F2, E2F3, and E2F4. Loss of E2F2 preferentially decreased CIT expression

and also counteracted 0.1nM R1881-mediated CIT induction (Figure 4E–F). These results identified a previously unrecognized role for E2F2 in CaP as a preferential determinant of CIT expression. Combining CIT overexpression with knock-down of E2F2 rescued the decrease in cell proliferation induced by loss of E2F2 (Figure 4G), confirming a role for CIT in E2F2 control over CaP cell proliferation. Furthermore, E2F2 overexpression increased cell viability both under FBS-supplemented growth conditions and under ADT (Figure 4H).

In view of this novel role for E2F2, we performed an RNA-Seq experiment to define E2F2-dependent CaP genes and to compare these to genes regulated by E2F1. Gene selection criteria and nomenclature used for E2F1/2-dependent gene isolation and qRT-PCR validation are shown in Supplementary Figure 1. Following E2F1-silencing, approximately 60 genes were up- or downregulated at the basal level, whereas E2F2 depletion led to 417 and 644 downregulated or upregulated genes respectively, suggesting a more pronounced effect of E2F2 on CaP cell biology (Supplementary Figure 5A). Moreover, comparing these E2F1- and E2F2-controlled genes revealed limited overlap only (range: 5–20) (Supplementary Figure 5B). MSigDB analyses for hallmark and oncogenic gene sets on E2F1- and E2F2-regulated gene signatures showed little or no overlap for genes whose basal expression was increased or decreased by E2F1/2 knock-out, respectively, supporting distinct roles for E2F1 and E2F2 in CaP (Supplementary Figure 5C, Supplementary Information Table 4). The number of growth-repressed and -induced genes following E2F2 or E2F1 knockdown ranged from 50 to 120. MSigDB analyses for hallmark and oncogenic gene sets showed a more pronounced but also incomplete overlap for E2F1- and E2F2- growth-regulated genes (Supplementary Figure 5D–F). Furthermore, the E2F1/2-dependent signatures behaved differently in GSEA between CRPC and localized treatment-naïve samples. Similar to genes that relied on CIT to maintain their expression, genes downregulated by E2F2 loss were strongly enriched in CRPC, underscoring the relevance of E2F2 to CRPC (Supplementary Figure 5F).

With regard to our working model, silencing Skp2 decreased CIT expression, which was counteracted by loss of p27, suggesting p27 mediates this effect. Loss of p27 increased CIT expression (Figure 5A). We then explored the possibility of physical interaction between CIT and p27, which was previously reported in normal mouse cells (36). In Co-IPs on LNCaP and VCaP cells, we found that an antibody against p27 also precipitated CIT, and did so most efficiently under conditions of 0.1 nM R1881 stimulation (Figure 5B). Co-IP for Skp2 served as positive control. These findings indicate that p27 and CIT interact to control CIT expression downstream of a novel E2F-Skp2-p27 signaling axis in CaP.

## CIT is a therapeutic target throughout CaP progression

We next examined CIT-dependence of CRPC lines reflecting different mechanisms of in vivo resistance to ADT such as castration as first-line androgen deprivation [C4–2 (40)], expression of ligand-independent AR variant ARv567es that is not responsive to ADT [R1-D567 (15)], resistance to sequential castration and enzalutamide [V16D, 49C$^{ENZR}$, 49F$^{ENZR}$ (16)], NEPC cell lines [42D$^{ENZR}$, 42F$^{ENZR}$ (16)], as well as AR-negative cell lines PC-3 and DU-145, which have also been proposed to model NEPC. siRNA-mediated silencing of CIT decreased viability of all CaP cell lines, irrespective of CaP stage or mechanism by

which CaP treatment resistance occurs (Figure 6A). In the enzalutamide-responsive CRPC lines C4–2 and V16D, enzalutamide treatment after CIT silencing decreased cell viability further than either treatment alone (Figure 6B). The impact of CIT loss on cell viability was comparable between Rb-mutant (DU145) and Rb-wild type cells (all other cells) (Figure 6A) and loss of Rb did not reverse the inhibitory effect of CIT on cell viability or CIT's growth-induction (Supplementary Figure 6A), suggesting that Rb, which can control E2F function, is not a major determinant of CIT's role. Doxycycline treatment of CRPC R1-D567 sublines that express doxycycline-inducible CIT-targeting shRNA or mice carrying R1-D567-shCIT xenografts led to decreased CaP cell viability in vitro and decreased CaP volumes and delayed CaP progression in vivo (Figure 6C). These findings confirm CIT is an important mediator of treatment-resistant CaP growth and a viable therapeutic target throughout CaP progression.

## CIT's kinase activity is critical for CaP cell proliferation and represents a druggable target

Because CIT is a serine/threonine kinase whose kinase action may represent a druggable target, we investigated further the contribution of its kinase moiety to CaP growth. While overexpression of wild-type CIT significantly increased the number of proliferating CaP cells, the same expression level of a kinase-dead mutant of CIT (K126A, CIT-KD) that abrogates its kinase activity (6) did not induce such proliferation (Figure 7A), demonstrating CIT kinase action is critical to CaP cell proliferation. Moreover, wild-type but not CIT-KD increased levels of phosphorylated MCL2, a CIT kinase substrate in in vitro assays (10, 41).

Together with reports that loss of CIT does not affect viability in mammals (7, 8), these findings imply that CIT's kinase function is an attractive target for CaP treatment. However, CIT is an "orphan kinase" for which no inhibitor has been developed (42). We queried the kinase targets for 243 kinase inhibitors that are either clinically approved or have previously been tested in humans (43) to determine whether the polypharmacology of kinase inhibitors can be exploited to target CIT activity. We identified 5 kinase inhibitors, apitolisib, tofacitinib, OTS-167, Y-39983, and dacomitinib (Figure 7B) with a reported CIT $EC_{50}$<100nM (43). In independent CIT in vitro kinase assays, we found the CIT IC50s to range from ~10nM for OTS-167 to above assay detection levels for other inhibitors (Figure 7B). We focused on the most potent of these inhibitors, OTS-167, originally identified as a MELK inhibitor (44). In dose-response studies, OTS-167 significantly reduced viability of ADT-naïve, CRPC, NEPC and AR-negative CaP cell lines at doses ranging from 5 to 100nM (Figure 7C, Supplementary Figure 6B). Noteworthy, apoptosis as measured by PARP cleavage was induced only at the higher OTS-167 dose in 2 representative treatment-resistant cell lines and in ADT-responsive LNCaP cells, suggesting that OTS-167 primarily inhibits CaP cell proliferation (Supplementary Figure 6C). In addition, OTS-167 prevented normal growth of patient-derived organoids (PDOs) generated from the CRPC orthotopic intrafemoral patient-derived xenograft, Prostate Cancer San Diego 1, PCSD1 (45, 46) (Figure 7D). PDO growth and differentiation involves CaP stem-cell mediated development of early spheroids (no lumen) that develop into mature, larger spheroids and cysts (lumen). After 72h, OTS-167 blocked cyst formation in 3D organoid culture, and led to accumulation of early/immature spheroid precursors that were smaller than those treated with vehicle, indicating that OTS-167 reduced cell proliferation and growth. At the low doses used,

OTS-167 induced a level of growth inhibition similar to that obtained after CIT knockout and moderately decreased CaP cell viability in combination with CIT depletion, indicating that a considerable portion of OTS-167's effects is mediated by CIT in CIT-expressing cells (Figure 7E). Decreases in cell viability caused by OTS-167 were rescued in part by CIT overexpression (Figure 7F).

### CIT substrates span diverse cellular functions including alternative splicing

CIT is a kinase but its substrates, whose phosphorylation status could serve as treatment-specific biomarkers of response to CIT inhibition, remain largely unknown. Some have been suggested by in vitro kinase assays, including myosin light chain 2 (MLC2) (10, 41) and histone 1 (10).

To start to define the extended landscape of CIT substrates in CaP cells, we employed mass spectrometry (MS). First, we performed CIT IP-MS in which we incorporated a phospho-enrichment step prior to MS and then analyzed phospho-peptides present in the phospho-enriched and flow-through CIT-specific IP fractions. Two independent experiments revealed 16 and 49 phospho-peptides derived from 13 and 26 proteins respectively. Second, we set up biotin-based proximity ligation assays coupled with MS (PLA-MS) to detect proteins that associate with wild-type CIT but not CIT-KD. In one PLA-MS assay, we screened wild-type CIT-interacting proteins for phosphorylation marks. In the other, we combined the PLA-MS assay with a phospho-enrichment step and determined the phospho-peptides present in the phospho-enriched and flow through fraction. These studies uncovered 13 and 122 phospho-peptides derived from 8 and 68 proteins respectively (Figure 8A). Phosphorylated proteins included several involved in cell division (e.g., CLASP1) and DNA damage repair (e.g., XPC), both associated with CIT action (7) (Supplemental Information Table 5) as well as histone 1 (10). CoIP studies confirmed interactions between CIT and representative MS hits such as MATR3 and THRAP3 (Figure 8B). In absence of specific antibodies targeting the phospho-Ser marks observed in THRAP3 and MATR3, we performed IPs using pSer-specific antibodies. Subsequent immunoblotting for MATR3 or THRAP3 showed diminished p-Ser immunoreactive signals after CIT silencing in LNCaP as well as VCaP cells, verifying CIT-dependent THRAP3 and MATR3 phosphorylation (Figure 8C). Serine phosphorylation levels of CIT substrates MLC2 and histone 3 (substrate in in vitro kinase assays of Figure 7B) served as control. Similar results were obtained in cells treated with 10nM OTS-167 (Figure 8D). Silencing of THRAP or MATR3 decreased CaP cell viability, mirroring the effect of loss of CIT (Figure 8E).

To determine the cellular processes mediated by the phosphorylated CIT interactors, we performed MSigDB curated gene set analyses (Supplemental Information Table 6). Enrichments related to RNA metabolism, processing and/or splicing in CIT-dependent phosphopeptides were returned in 2 studies and all experiments isolated phosphorylations in proteins implicated in these processes. Closer examination revealed that 37 of 100 identified CIT-dependent phosphorylated marks occurred in proteins involved in RNA processing, metabolism or splicing. We verified that 50% of phosphorylated CIT interactors were present in the Spliceosome Database (47) (Figure 8F). We then reanalyzed our CIT-dependent RNA-Seq data for evidence of alternative splicing using rMATS (48). We

noted 897 CIT-dependent splicing events, the majority of which were skipped exon events (Figure 8G, validation of representative skipped exon events in Supplementary Figure 7). Comparison of genes that undergo CIT-dependent splicing events and genes impacted by alternative splicing in the progression from benign prostate to treatment-resistant CaP (14), showed significant overlap. Enrichments became more pronounced in CRPC and NEPC and were most significant for skipped exon events (Figure 8H). These results provide further insights into how CIT impacts CaP cell proliferation and suggest that events previously unrecognized to be CIT-dependent, such as alternative splicing, contribute to CIT-mediated CaP progression (Figure 8I).

## Discussion

We isolated CIT as a novel pivotal regulator of CaP progression. CIT was preferentially involved in control of malignant over benign cell proliferation, suggesting a suitable therapeutic window for CIT-targeting therapies. Importantly, CIT is also a feasible target because mammals with germline loss of CIT or loss-of-function CIT mutations are viable (7, 8) and CIT is not essential for normal postnatal growth (13, 49). Moreover, CIT's genetic inactivation in a meduloblastoma mice model reduced tumor growth without any side effects (50).

Our studies uncovered a critical role for CIT in CaP cell proliferation. Results support the well-recognized role for CIT role in cytokinesis but isolated also a role for CIT in interphase. CIT controlled CaP interphase progression and its expression levels depended on cell cycle stage. These findings are consistent with cell cycle-dependent CIT expression patterns in hepatocytes (51) and fit with the E2F-Skp2-p27 dependence of CIT expression. CIT's role as determinant of CaP cell proliferation, which we found to occur irrespective of CaP cells' AR expression status or Rb-ness, does not rule out that CIT impacts CaP progression via other cellular processes. Novel CIT-dependent EMT roles were shown in our in vitro (enhanced EMT marker expression) and in vivo (cachexia without overt localized CaP growth) tumorigenesis assays as well as RNA-Seq studies (MSigDB). Our MS data also indicated that a significant fraction of the newly isolated in vivo CIT substrates function in RNA-binding, metabolism, and splicing. The latter process is a well-known contributor to treatment resistance and aggressive clinical CaP progression (14) that is tightly controlled by phosphorylation (52) and cell cycle stage progression (53), but remains poorly understood mechanistically.

The relevance of CIT to clinical CaP progression observed in our GSEA and PTCA analyses fits with the induction of its expression by growth stimuli that feeds forward to control CaP growth, and its overexpression during CaP progression. When mimicked experimentally CIT overexpression induced pluripotency and promoted CaP growth even under conditions intended to restrict growth. CIT expression was controlled by a novel E2F2-Skp2-p27 signaling axis, whose CaP expression patterns (higher E2F, higher Skp2, lower p27 expression (54–56)) and CaP relevance are similar to that observed for CIT. Most studies of E2F action in CaP have focused on E2F1, whose expression increases with clinical CaP progression (57). Our siRNA screen, RNA-Seq, MSigDB and GSEA analyses indicated E2F2 had a more prominent effect on growth-induced CIT expression and was

most relevant to CRPC, uncovering an entirely novel role for E2F2 in CaP distinct from E2F1. Because E2F activity in general impacts Skp2 and p27, our findings imply also that other factors may contribute to E2F2's preferential control over CIT.

Although p27 is one of the better-known substrates of the Skp2 E3 ligase, interpretation of its role in control of CIT (ubiquitination) may be less straight-forward. p27 is best known as a tumor suppressor, which inhibits cyclin-CDK complex activities. More recently, a CDK-independent oncogenic role has been described for a form of p27 that is unable to interact with CDKs/cyclin (p27-CK). p27-CK is located in the cytoplasm, in contrast to the nuclear location of the CDK-interacting form of p27 (58–60). In CaP, the role for different fractions of the p27 cellular pool is not yet clear. Although previous work suggests both cytoplasmic and nuclear fractions of p27 exist in clinical CaP, decreased p27 expression was associated with poor CaP outcome irrespective of p27 location (56). Because p27-CK, which cannot interact with CDK/cyclins, is not degraded by Skp2 (58, 59), our work points to another novel role for p27 in CIT-dependent CaP growth. Our working model indicates p27-controlled proteosome-mediated CIT ubiquitination occurs in the absence of growth stimulation, the molecular regulation of which will be important to explore. That CIT-p27 interaction is more pronounced after growth-stimulation seems counterintuitive but is consistently observed. Whether growth-induction and suppression lead CIT to interact with functionally different p27 populations (61) or cause cell cycle-dependent different signal transductions to control p27 action (62) will need to be examined.

As a mitotic kinase, CIT differs functionally from targets for current standard of care treatments, such as ADT (targets AR) or chemotherapy (targets microtubule stability), and may thus bypass the cellular rewiring that causes drug resistance under such treatments. Although low androgen growth stimulation can activate CIT in AR-positive cells, CIT activation in and of itself does not rely on the presence or activity of AR. The latter is supported by our PCTA analyses and CIT induction after serum restoration, which our ongoing studies show also in AR-negative models. CIT-dependent genes remain highly expressed or enriched in treatment-resistant CaP. In contrast, expression of genes directly controlled by AR, the default target for treatment for metastatic CaP, decreased in CRPC compared to treatment-naïve CaP (17, 33, 34). Along with our data showing potent inhibitory effects on CaP growth after CIT silencing or inactivation in CPRC and NEPC models, these findings support CIT as a novel driver of CaP progression and promising target for mechanistically novel therapies.

CIT's reliance on its kinase domain to maintain CaP cell proliferation provides a potentially druggable entity and further increases its appeal as therapeutic target. Indeed, overexpression of a kinase-dead version of CIT, even in cells that still express wild-type CIT, decreased significantly cell viability. Our analyses show that the polypharmacology that is increasingly being recognized for kinase inhibitors (43, 63), most of which inhibit multiple kinases, provides opportunities for drug repurposing to inhibit CIT. OTS-167, the drug we identified as the most potent CIT inhibitor, was originally developed as a MELK inhibitor (44), which has been questioned because it has effects also on cells that do not express MELK (64). Even though OTS-167 is not entirely specific for CIT, we found that a substantial fraction of OTS-167 action is mediated via CIT in CIT-expressing cells, and that OTS-167 inhibits

the growth of CaP models representing different stages of CaP progression and forms of treatment resistance. Publically available kinase inhibitor polypharmacology data (43) listed 5 drugs with a CIT $EC_{50}$<100nM; our in vitro kinase assay validation returned low CIT $IC_{50}$ values for only 2 inhibitors (Y-39983 and OTS-167). These discrepancies reflect the difference in what is being measured by both parameters: $EC_{50}$ is the concentration of a drug that gives half-maximal response whereas $IC_{50}$ is the concentration of an inhibitor where the response is reduced by half. Our in vitro kinase data in Figure 7 confirm that only OTS-167 and Y-39983 completely inhibit CIT as measured via both parameters. These data support the feasibility of drugging CIT. Our isolation of the in vivo CaP CIT interactome and its phosphorylation landscape provide the first glimpses of the manner in which the activity of this poorly characterized kinase may control aggressive CaP behavior and progression. Its isolation meets another important condition for ultimate applicability of CIT inhibition, namely the potential as a treatment-specific biomarker of response. In CaP, potentially effective kinase-inhibiting drugs such as the multikinase inhibitor lestaurtinib/CEP-701 have been abandoned despite their promise as CaP therapeutics because of inadequate biomarkers to monitor treatment response (9, 65, 66). Verifying the phosphorylation status of CIT substrates or CIT interactions in circulating tumor cells or tissues from CRPC patients may overcome such limitations for CIT-targeting therapies. Follow-up studies are needed to validate these findings further, define the broader spectrum of CIT substrates across cell cycle stages, characterize CITs substrate recognition motif, and determine the relevance of CIT-controlled phosphomarks for aggressive CaP behavior.

In combination, our studies provide novel insights in the molecular regulation of CaP cell proliferation that may be exploited to address one of the most critical barriers to improving CaP survival: new treatments that are functionally diverse and bypass treatment resistance.

## Supplementary Material

Refer to Web version on PubMed Central for supplementary material.

## Acknowledgments:

The authors thank Dr. Cassandra Talerico for review of the manuscript, Cleveland Clinic Enterprise Creative services for assistance with Figure 8I, and Heemers lab members for helpful discussions. These studies were supported by NIH NCI grants CA166440 (HVH), CA248048 (HVH), CA232979 (SL) and U24CA274159 (SL), a Pilot Research Award from the Case Comprehensive Cancer Center Support Grant (HVH), a Falk Medical Research Trust Catalyst Award (HVH) and a VeloSano 5 Pilot Research Award (HVH). The Fusion Lumos instrument was purchased via an NIH shared instrument grant, 1S10OD023436-01.

### Financial support:

These studies were supported by NIH NCI grants CA166440 (HVH), CA248048 (HVH), CA232979 (SL) and U24CA274159 (SL), a Pilot Research Award from the Case Comprehensive Cancer Center Support Grant (HVH), a Falk Medical Research Trust Catalyst Award (HVH) and a VeloSano 5 Pilot Research Award (HVH). The Fusion Lumos instrument was purchased via an NIH shared instrument grant, 1S10OD023436-01.

## References

1. Siegel RL, Miller KD, Wagle NS, Jemal A. Cancer statistics, 2023. CA Cancer J Clin. 2023;73(1):17–48. [PubMed: 36633525]

2. Dai C, Dehm SM, Sharifi N. Targeting the Androgen Signaling Axis in Prostate Cancer. J Clin Oncol. 2023:JCO2300433.
3. Beltran H, Prandi D, Mosquera JM, Benelli M, Puca L, Cyrta J, et al. Divergent clonal evolution of castration-resistant neuroendocrine prostate cancer. Nat Med. 2016;22(3):298–305. [PubMed: 26855148]
4. Schaeffer EM, Srinivas S, Adra N, An Y, Barocas D, Bitting R, et al. NCCN Guidelines(R) Insights: Prostate Cancer, Version 1.2023. J Natl Compr Canc Netw. 2022;20(12):1288–98. [PubMed: 36509074]
5. Ben-Salem S, Venkadakrishnan VB, Heemers HV. Novel insights in cell cycle dysregulation during prostate cancer progression. Endocr Relat Cancer. 2021;28(6):R141–R55. [PubMed: 33830069]
6. Madaule P, Eda M, Watanabe N, Fujisawa K, Matsuoka T, Bito H, et al. Role of citron kinase as a target of the small GTPase Rho in cytokinesis. Nature. 1998;394(6692):491–4. [PubMed: 9697773]
7. D'Avino PP. Citron kinase - renaissance of a neglected mitotic kinase. J Cell Sci. 2017;130(10):1701–8. [PubMed: 28468989]
8. Bianchi FT, Gai M, Berto GE, Di Cunto F. Of rings and spines: The multiple facets of Citron proteins in neural development. Small GTPases. 2017:1–9. [PubMed: 27715453]
9. Venkadakrishnan VB, DePriest AD, Kumari S, Senapati D, Ben-Salem S, Su Y, et al. Protein Kinase N1 control of androgen-responsive serum response factor action provides rationale for novel prostate cancer treatment strategy. Oncogene. 2019.
10. Di Cunto F, Calautti E, Hsiao J, Ong L, Topley G, Turco E, et al. Citron rho-interacting kinase, a novel tissue-specific ser/thr kinase encompassing the Rho-Rac-binding protein Citron. J Biol Chem. 1998;273(45):29706–11. [PubMed: 9792683]
11. Camera P, Schubert V, Pellegrino M, Berto G, Vercelli A, Muzzi P, et al. The RhoA-associated protein Citron-N controls dendritic spine maintenance by interacting with spine-associated Golgi compartments. EMBO Rep. 2008;9(4):384–92. [PubMed: 18309323]
12. Furuyashiki T, Fujisawa K, Fujita A, Madaule P, Uchino S, Mishina M, et al. Citron, a Rho-target, interacts with PSD-95/SAP-90 at glutamatergic synapses in the thalamus. J Neurosci. 1999;19(1):109–18. [PubMed: 9870943]
13. Di Cunto F, Imarisio S, Hirsch E, Broccoli V, Bulfone A, Migheli A, et al. Defective neurogenesis in citron kinase knockout mice by altered cytokinesis and massive apoptosis. Neuron. 2000;28(1):115–27. [PubMed: 11086988]
14. Zhang D, Hu Q, Liu X, Ji Y, Chao HP, Liu Y, et al. Intron retention is a hallmark and spliceosome represents a therapeutic vulnerability in aggressive prostate cancer. Nat Commun. 2020;11(1):2089. [PubMed: 32350277]
15. Nyquist MD, Li Y, Hwang TH, Manlove LS, Vessella RL, Silverstein KA, et al. TALEN-engineered AR gene rearrangements reveal endocrine uncoupling of androgen receptor in prostate cancer. Proc Natl Acad Sci U S A. 2013;110(43):17492–7. [PubMed: 24101480]
16. Bishop JL, Thaper D, Vahid S, Davies A, Ketola K, Kuruma H, et al. The Master Neural Transcription Factor BRN2 Is an Androgen Receptor-Suppressed Driver of Neuroendocrine Differentiation in Prostate Cancer. Cancer Discov. 2017;7(1):54–71. [PubMed: 27784708]
17. Liu S, Kumari S, Hu Q, Senapati D, Venkadakrishnan VB, Wang D, et al. A comprehensive analysis of coregulator recruitment, androgen receptor function and gene expression in prostate cancer. Elife. 2017;6.
18. McNair C, Urbanucci A, Comstock CE, Augello MA, Goodwin JF, Launchbury R, et al. Cell cycle-coupled expansion of AR activity promotes cancer progression. Oncogene. 2017;36(12):1655–68. [PubMed: 27669432]
19. Katz Y, Wang ET, Silterra J, Schwartz S, Wong B, Thorvaldsdottir H, et al. Quantitative visualization of alternative exon expression from RNA-seq data. Bioinformatics. 2015;31(14):2400–2. [PubMed: 25617416]
20. You S, Knudsen BS, Erho N, Alshalalfa M, Takhar M, Al-Deen Ashab H, et al. Integrated Classification of Prostate Cancer Reveals a Novel Luminal Subtype with Poor Outcome. Cancer Res. 2016;76(17):4948–58. [PubMed: 27302169]

21. Liberzon A, Birger C, Thorvaldsdottir H, Ghandi M, Mesirov JP, Tamayo P. The Molecular Signatures Database (MSigDB) hallmark gene set collection. Cell Syst. 2015;1(6):417–25. [PubMed: 26771021]
22. Ben-Salem S, Hu Q, Liu Y, Alshalalfa M, Zhao X, Wang I, et al. Diversity in Androgen Receptor Action Among Treatment-naive Prostate Cancers Is Reflected in Treatment Response Predictions and Molecular Subtypes. Eur Urol Open Sci. 2020;22:34–44. [PubMed: 33299986]
23. Sharma NL, Massie CE, Ramos-Montoya A, Zecchini V, Scott HE, Lamb AD, et al. The androgen receptor induces a distinct transcriptional program in castration-resistant prostate cancer in man. Cancer Cell. 2013;23(1):35–47. [PubMed: 23260764]
24. Arriaga JM, Panja S, Alshalalfa M, Zhao J, Zou M, Giacobbe A, et al. A MYC and RAS co-activation signature in localized prostate cancer drives bone metastasis and castration resistance. Nat Cancer. 2020;1(11):1082–96. [PubMed: 34085047]
25. Mohammed H, Taylor C, Brown GD, Papachristou EK, Carroll JS, D'Santos CS. Rapid immunoprecipitation mass spectrometry of endogenous proteins (RIME) for analysis of chromatin complexes. Nat Protoc. 2016;11(2):316–26. [PubMed: 26797456]
26. Cox J, Hein MY, Luber CA, Paron I, Nagaraj N, Mann M. Accurate proteome-wide label-free quantification by delayed normalization and maximal peptide ratio extraction, termed MaxLFQ. Mol Cell Proteomics. 2014;13(9):2513–26. [PubMed: 24942700]
27. Branon TC, Bosch JA, Sanchez AD, Udeshi ND, Svinkina T, Carr SA, et al. Efficient proximity labeling in living cells and organisms with TurboID. Nature Biotechnology. 2018;36:880.
28. Drost J, Artegiani B, Clevers H. The Generation of Organoids for Studying Wnt Signaling. Methods Mol Biol. 2016;1481:141–59. [PubMed: 27590160]
29. Denmeade SR, Isaacs JT. Bipolar androgen therapy: the rationale for rapid cycling of supraphysiologic androgen/ablation in men with castration resistant prostate cancer. The Prostate. 2010;70(14):1600–7. [PubMed: 20607766]
30. Sedelaar JP, Isaacs JT. Tissue culture media supplemented with 10% fetal calf serum contains a castrate level of testosterone. Prostate. 2009;69(16):1724–9. [PubMed: 19676093]
31. Zhau HY, Chang SM, Chen BQ, Wang Y, Zhang H, Kao C, et al. Androgen-repressed phenotype in human prostate cancer. Proc Natl Acad Sci U S A. 1996;93(26):15152–7. [PubMed: 8986779]
32. Liu J, Dou J, Wang W, Liu H, Qin Y, Yang Q, et al. High expression of citron kinase predicts poor prognosis of prostate cancer. Oncol Lett. 2020;19(3):1815–23. [PubMed: 32194675]
33. Tomlins SA, Mehra R, Rhodes DR, Cao X, Wang L, Dhanasekaran SM, et al. Integrative molecular concept modeling of prostate cancer progression. Nat Genet. 2007;39(1):41–51. [PubMed: 17173048]
34. Stanbrough M, Bubley GJ, Ross K, Golub TR, Rubin MA, Penning TM, et al. Increased expression of genes converting adrenal androgens to testosterone in androgen-independent prostate cancer. Cancer Res. 2006;66(5):2815–25. [PubMed: 16510604]
35. Swartz KL, Wood SN, Murthy T, Ramirez O, Qin G, Pillai MM, et al. E2F-2 Promotes Nuclear Condensation and Enucleation of Terminally Differentiated Erythroblasts. Mol Cell Biol. 2017;37(1).
36. Serres MP, Kossatz U, Chi Y, Roberts JM, Malek NP, Besson A. p27(Kip1) controls cytokinesis via the regulation of citron kinase activation. J Clin Invest. 2012;122(3):844–58. [PubMed: 22293177]
37. Hofman K, Swinnen JV, Verhoeven G, Heyns W. E2F activity is biphasically regulated by androgens in LNCaP cells. Biochem Biophys Res Commun. 2001;283(1):97–101. [PubMed: 11322773]
38. Assoian RK, Yung Y. A reciprocal relationship between Rb and Skp2: implications for restriction point control, signal transduction to the cell cycle and cancer. Cell Cycle. 2008;7(1):24–7. [PubMed: 18196971]
39. Bauzon F, Zhu L. Racing to block tumorigenesis after pRb loss: an innocuous point mutation wins with synthetic lethality. Cell Cycle. 2010;9(11):2118–23. [PubMed: 20505340]
40. Wu HC, Hsieh JT, Gleave ME, Brown NM, Pathak S, Chung LW. Derivation of androgen-independent human LNCaP prostatic cancer cell sublines: role of bone stromal cells. Int J Cancer. 1994;57(3):406–12. [PubMed: 8169003]

41. Yamashiro S, Totsukawa G, Yamakita Y, Sasaki Y, Madaule P, Ishizaki T, et al. Citron kinase, a Rho-dependent kinase, induces di-phosphorylation of regulatory light chain of myosin II. Mol Biol Cell. 2003;14(5):1745–56. [PubMed: 12802051]
42. Carles F, Bourg S, Meyer C, Bonnet P. PKIDB: A Curated, Annotated and Updated Database of Protein Kinase Inhibitors in Clinical Trials. Molecules. 2018;23(4).
43. Klaeger S, Heinzlmeir S, Wilhelm M, Polzer H, Vick B, Koenig PA, et al. The target landscape of clinical kinase drugs. Science. 2017;358(6367).
44. Chung S, Suzuki H, Miyamoto T, Takamatsu N, Tatsuguchi A, Ueda K, et al. Development of an orally-administrative MELK-targeting inhibitor that suppresses the growth of various types of human cancer. Oncotarget. 2012;3(12):1629–40. [PubMed: 23283305]
45. Godebu E, Muldong M, Strasner A, Wu CN, Park SC, Woo JR, et al. PCSD1, a new patient-derived model of bone metastatic prostate cancer, is castrate-resistant in the bone-niche. J Transl Med. 2014;12:275. [PubMed: 25278011]
46. Raheem O, Kulidjian AA, Wu C, Jeong YB, Yamaguchi T, Smith KM, et al. A novel patient-derived intra-femoral xenograft model of bone metastatic prostate cancer that recapitulates mixed osteolytic and osteoblastic lesions. J Transl Med. 2011;9:185. [PubMed: 22035283]
47. Cvitkovic I, Jurica MS. Spliceosome database: a tool for tracking components of the spliceosome. Nucleic Acids Res. 2013;41(Database issue):D132–41. [PubMed: 23118483]
48. Shen S, Park JW, Lu ZX, Lin L, Henry MD, Wu YN, et al. rMATS: robust and flexible detection of differential alternative splicing from replicate RNA-Seq data. Proc Natl Acad Sci U S A. 2014;111(51):E5593–601. [PubMed: 25480548]
49. Bianchi FT, Tocco C, Pallavicini G, Liu Y, Verni F, Merigliano C, et al. Citron Kinase Deficiency Leads to Chromosomal Instability and TP53-Sensitive Microcephaly. Cell Rep. 2017;18(7):1674–86. [PubMed: 28199840]
50. Pallavicini G, Sgro F, Garello F, Falcone M, Bitonto V, Berto GE, et al. Inactivation of Citron Kinase Inhibits Medulloblastoma Progression by Inducing Apoptosis and Cell Senescence. Cancer Res. 2018;78(16):4599–612. [PubMed: 29921697]
51. Liu H, Di Cunto F, Imarisio S, Reid LM. Citron kinase is a cell cycle-dependent, nuclear protein required for G2/M transition of hepatocytes. J Biol Chem. 2003;278(4):2541–8. [PubMed: 12411428]
52. Naro C, Sette C. Phosphorylation-mediated regulation of alternative splicing in cancer. Int J Cell Biol. 2013;2013:151839. [PubMed: 24069033]
53. Dominguez D, Tsai YH, Weatheritt R, Wang Y, Blencowe BJ, Wang Z. An extensive program of periodic alternative splicing linked to cell cycle progression. Elife. 2016;5.
54. Network TCGAR. The Molecular Taxonomy of Primary Prostate Cancer. Cell. 2015;163(4):1011–25. [PubMed: 26544944]
55. Robinson D, Van Allen EM, Wu YM, Schultz N, Lonigro RJ, Mosquera JM, et al. Integrative clinical genomics of advanced prostate cancer. Cell. 2015;161(5):1215–28. [PubMed: 26000489]
56. Ananthanarayanan V, Deaton RJ, Amatya A, Macias V, Luther E, Kajdacsy-Balla A, et al. Subcellular localization of p27 and prostate cancer recurrence: automated digital microscopy analysis of tissue microarrays. Hum Pathol. 2011;42(6):873–81. [PubMed: 21292307]
57. Davis JN, Wojno KJ, Daignault S, Hofer MD, Kuefer R, Rubin MA, et al. Elevated E2F1 inhibits transcription of the androgen receptor in metastatic hormone-resistant prostate cancer. Cancer Res. 2006;66(24):11897–906. [PubMed: 17178887]
58. Agarwal A, Mackenzie RJ, Besson A, Jeng S, Carey A, LaTocha DH, et al. BCR-ABL1 promotes leukemia by converting p27 into a cytoplasmic oncoprotein. Blood. 2014;124(22):3260–73. [PubMed: 25293778]
59. Besson A, Gurian-West M, Chen X, Kelly-Spratt KS, Kemp CJ, Roberts JM. A pathway in quiescent cells that controls p27Kip1 stability, subcellular localization, and tumor suppression. Genes Dev. 2006;20(1):47–64. [PubMed: 16391232]
60. Serres MP, Zlotek-Zlotkiewicz E, Concha C, Gurian-West M, Daburon V, Roberts JM, et al. Cytoplasmic p27 is oncogenic and cooperates with Ras both in vivo and in vitro. Oncogene. 2011;30(25):2846–58. [PubMed: 21317921]

61. Lee JG, Kay EP. Two populations of p27 use differential kinetics to phosphorylate Ser-10 and Thr-187 via phosphatidylinositol 3-Kinase in response to fibroblast growth factor-2 stimulation. J Biol Chem. 2007;282(9):6444–54. [PubMed: 17209046]

62. Sa G, Stacey DW. P27 expression is regulated by separate signaling pathways, downstream of Ras, in each cell cycle phase. Exp Cell Res. 2004;300(2):427–39. [PubMed: 15475007]

63. Davis MI, Hunt JP, Herrgard S, Ciceri P, Wodicka LM, Pallares G, et al. Comprehensive analysis of kinase inhibitor selectivity. Nat Biotechnol. 2011;29(11):1046–51. [PubMed: 22037378]

64. Settleman J, Sawyers CL, Hunter T. Challenges in validating candidate therapeutic targets in cancer. Elife. 2018;7.

65. Collins C, Carducci MA, Eisenberger MA, Isaacs JT, Partin AW, Pili R, et al. Preclinical and clinical studies with the multi-kinase inhibitor CEP-701 as treatment for prostate cancer demonstrate the inadequacy of PSA response as a primary endpoint. Cancer Biol Ther. 2007;6(9):1360–7. [PubMed: 17786033]

66. Venkadakrishnan VB, Ben-Salem S, Heemers HV. AR-dependent phosphorylation and phospho-proteome targets in prostate cancer. Endocr Relat Cancer. 2020;27(6):R193–R210. [PubMed: 32276264]

## Significance statement

The poorly characterized protein kinase citron kinase is a therapeutic target in prostate cancer that drives tumor growth by regulating diverse substrates, which control several hallmarks of aggressive prostate cancer progression.

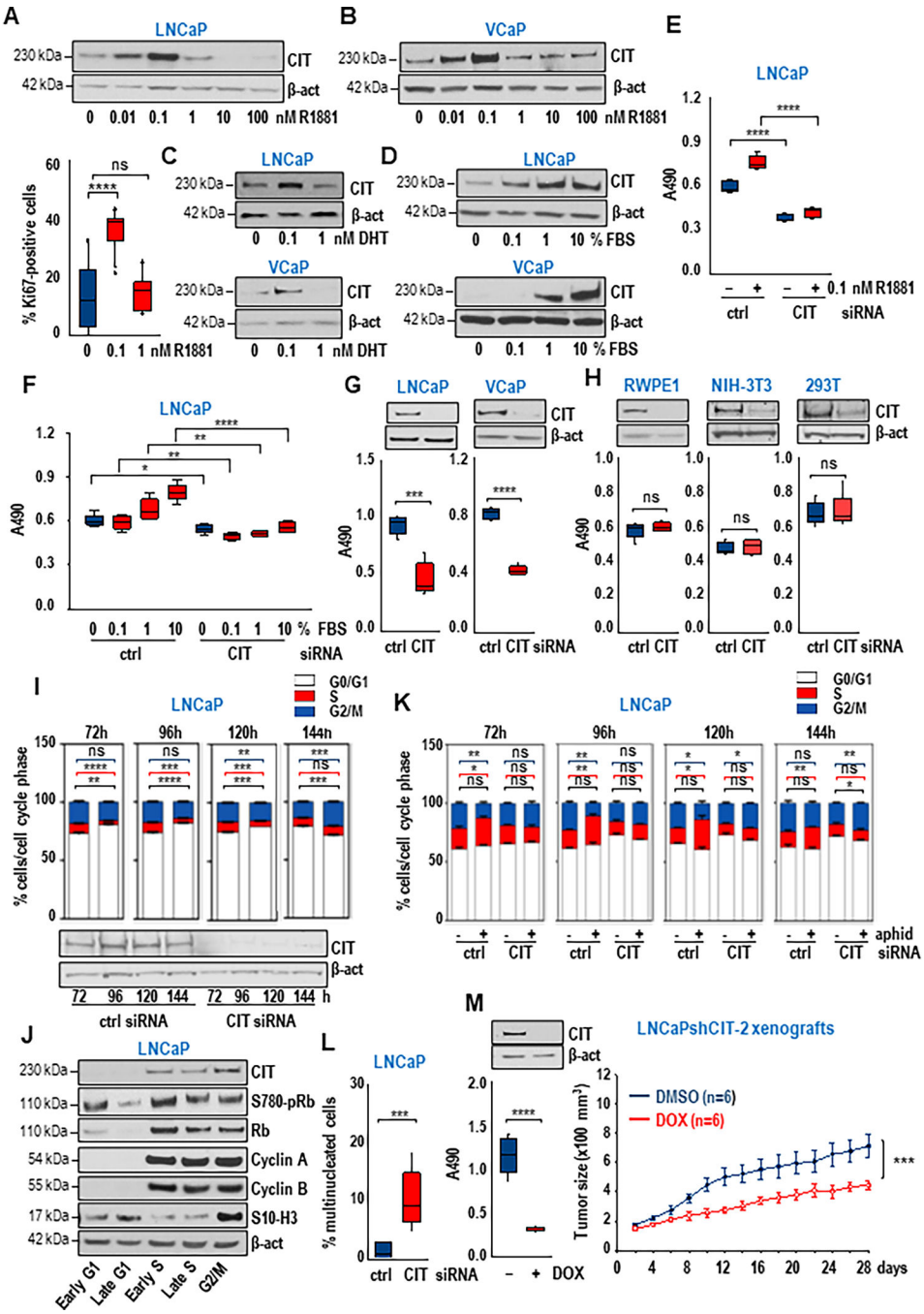


**Figure 1. CIT is a key regulator of CaP cell proliferation.**

(**A**) LNCaP cells were treated with increasing doses of R1881 for 48h. CIT and β-actin expression were analyzed by western blotting (top). In parallel, 96h after treatment, Ki67 immunofluorescent staining was done and nuclei counterstained with DAPI. Percentage of Ki67-positive cells was recorded (bottom). (**B**) VCaP cells were treated with R1881 for 48h and analyzed as under A (top). **(C)** LNCaP and VCaP cells were treated with indicated doses of dihydrotestosterone (DHT) for 48h and analyzed by western blotting for CIT and β-actin. (**D**) LNCaP and VCaP cells were treated with increasing doses of FBS for 2

days after overnight serum starvation. Cell lysates were analyzed by western blotting for CIT and β-actin. **(E, F)** LNCaP cells were transfected with siRNA targeting CIT (CIT) or control siRNA (ctrl). Two days later, cells were treated with 0.1nM R1881 for 96h or vehicle (ethanol) (E) or serum-starved for 24h and treated with increasing doses of FBS for 48h (F). Cell viability was assessed using an MTS assay read at 490 nm in quintuplicate. **(G)** LNCaP and VCaP cells were transfected with CIT or control (ctrl) siRNA. At 96h after transfection, cell viability was evaluated by MTS assay in quintuplicate (bottom). CIT and β-actin expression were analyzed by western blotting (top). **(H)** RWPE1, NIH-3T3 and 293T cells were transfected and assayed as under G. **(I)** Cells were transfected as under G. Cell cycle was evaluated after 72h, 96h, 120h or 144h by propidium iodide cell sorting. Percentage of cells in G0/G1, S, and G2/M phase is shown (in triplicate). Blue, red and black lines compare control vs CIT siRNA-transfected cells in G2/M, S and G0/1 phase, respectively. **(J)** LNCaP cells were pharmacologically enriched in early G1, late G1, early S, late S and G2/M phase for 24h. Phospho-Rb (S780-RB), Rb, cyclin A, cyclin B1, phospho-histone 3 (S10-H3) and β-actin were analyzed via western blotting. **(K)** LNCaP cells were transfected with siRNA targeting CIT (CIT) or control (ctrl) siRNA. 72, 96, 120 or 144h after transfection, cells were treated with 2μg/mL aphidicolin (aphid) for 24h. Cell cycle was evaluated as under I. **(L)** Cells were transfected as under G. At 96h after transfection, multinucleation was analyzed by immunofluorescence staining for the cell membrane marker $Na^+/K^+$ ATPase and counterstaining with nuclear marker stain DAPI. Percentage of multinucleated cells is shown. **(M)** LNCaP cells that express doxycycline-inducible shRNA targeting CIT #2 (Supplementary Figure 2) were treated with 1mg/ml doxycycline (DOX) or vehicle (DMSO) for 96h. Cell viability was evaluated as above (left panel). Cells were grafted subcutaneously in nude mice. Once xenografts reached $100mm^3$, animals were randomized to doxycycline (DOX, 200μg/ml, n=6, red) or vehicle (DMSO, n=6, blue). Tumor volumes were measured every other day for 28 days. *p<0.05, **p<0.01, ***p<0.001, and ****p<0.0001. Panels A, E, F, G, H, I, J, L, M (left): t-test, Panel M (right): 2-way ANOVA. Data are represented as means ±SEM. ns, non-significant. β-act, β-actin.

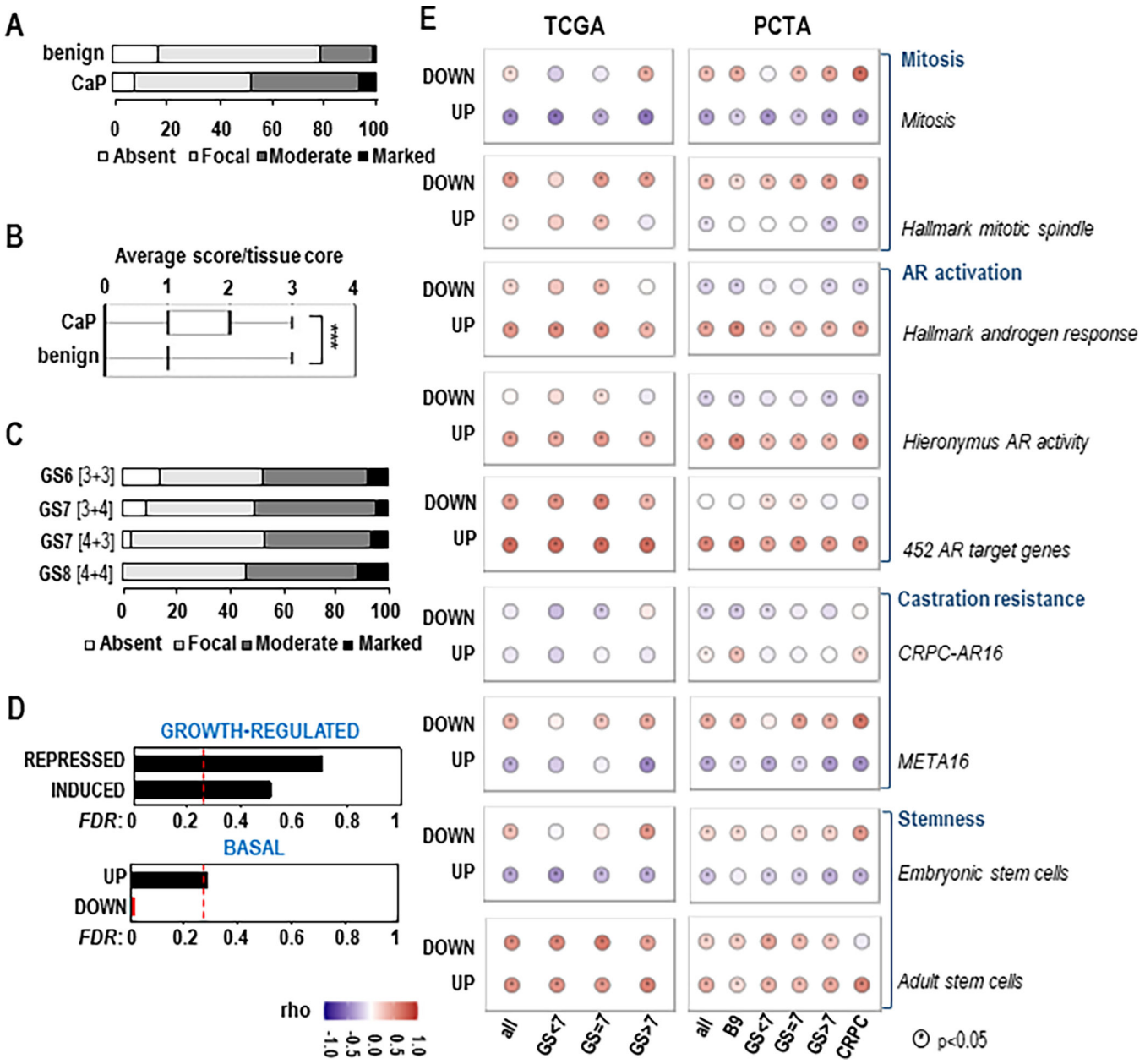


**Figure 2. Clinical and translational relevance of CIT during CaP progression.**

**(A)** Percentage of TMA cores with absent, focal, moderate or marked CIT immunohistochemical staining. **(B)** Average CIT expression score per tissue core in benign versus CaP tissues. *** p<0.001, t test. Box plots represent mean +/− SEM. (**C**) Percentage of cores with Gleason score (GS) of 6 (3+3), 7 (3+4 and 4+3), or 8 (4+4) with absent, focal, moderate or marked CIT immunohistochemical staining. **(D)** GSEA analysis of growth-regulated and basal CIT-dependent gene signatures, comparing CRPC and treatment-naïve CaP (GSE32269). Black bars, no significant enrichment; red bars, significant positive enrichment in CRPC compared to treatment-naïve CaP. Red dashed line: FDR<0.25, considered significant. (**E**) The PCTA web tool was used to mine PCTA and TCGA gene expression data by CaP subtype information based on GS and metastasis status. The

basal CIT-dependent gene signatures were analyzed in the PCTA correlation view analysis function against publically available signatures relevant to mitosis, AR activation, castration resistance and stemness, which are described in the Materials and Methods section. The correlation coefficient and p value derived from each PCTA analysis were recorded and represented graphically using R. * correlation with significance set at $p<0.05$ in PCTA. Up/down, up- or downregulated upon CIT silencing; B9, benign; all, all tissues.

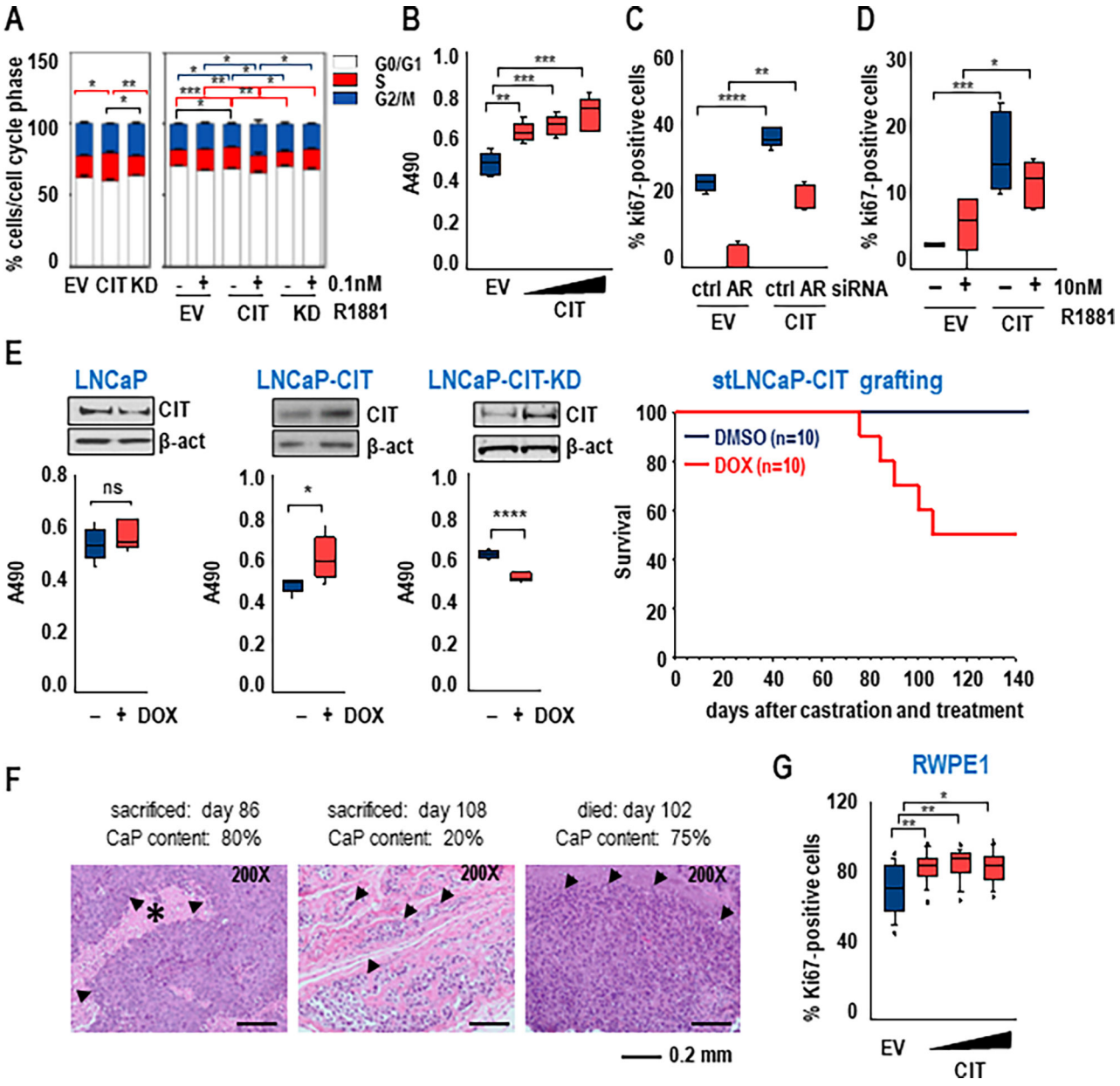


**Figure 3. CIT overexpression drives overcomes CaP growth restriction.**

(**A**) Percentage of LNCaP cells in G1, S, or G2/M phase as determined by propidium iodide assays 96h after transient transfection with an expression construct encoding CIT (CIT), kinase-dead CIT (KD) or empty vector (EV). Cells were grown in FBS-supplemented conditions (left) or treated with 0.1nM R1881 or vehicle (ethanol) (right). Black, red and blue lines compare G0/G1, S phase and G2/M phase. (**B**) LNCaP cells were transfected with increasing amounts of CIT or EV. Four days later, a cell viability assay reading at 490nM (in quintuplicate) was performed. (**C**) LNCaP cells were transfected with siRNA targeting AR or control siRNA (ctrl). Two days later, cells were transiently transfected with CIT or EV. Two days later, cell proliferation was analyzed via Ki67 staining and percentage of Ki67-positive cells was recorded. (**D**) LNCaP cells were transiently transfected with

CIT or EV. Two days later, cells were treated with 10nM R1881 (+) or vehicle (−) followed by Ki67 staining as above. (**E**) Parental (left) and isogenic LNCaP cells that stably express doxycycline-inducible CIT (middle) or CIT-KD were treated with 1μg/ml doxycycline (DOX) or vehicle (DMSO) for 96h, followed by an MTS assay read at 490nm (in quintuplicate).The LNCaP subline allowing for inducible CIT expression was grafted in castrated mice, which were randomized to immediate doxycycline treatment (DOX, 20μmg/L in drinking water, n=10) or vehicle (DMSO, n=10). Survival curve detailing animals that died or had to be sacrificed before the study end point (140 days) (right). (**F**) H&E staining on tissues from CaP-bearing animals from D (right panel), confirming presence of adenocarcinoma (arrows) in dox-treated mice that had to sacrificed at days 86, 108 or died at day 102 (bottom panel). *, area of necrosis. (**G**) RWPE1 cells were transfected with increasing amounts of CIT or with EV. Four days later, cell proliferation was analyzed via Ki67 staining. *p<0.05,**p<0.01, ***p< 0.001, and ****p<0.0001, t-test. Box plots reflect mean ±SEM.

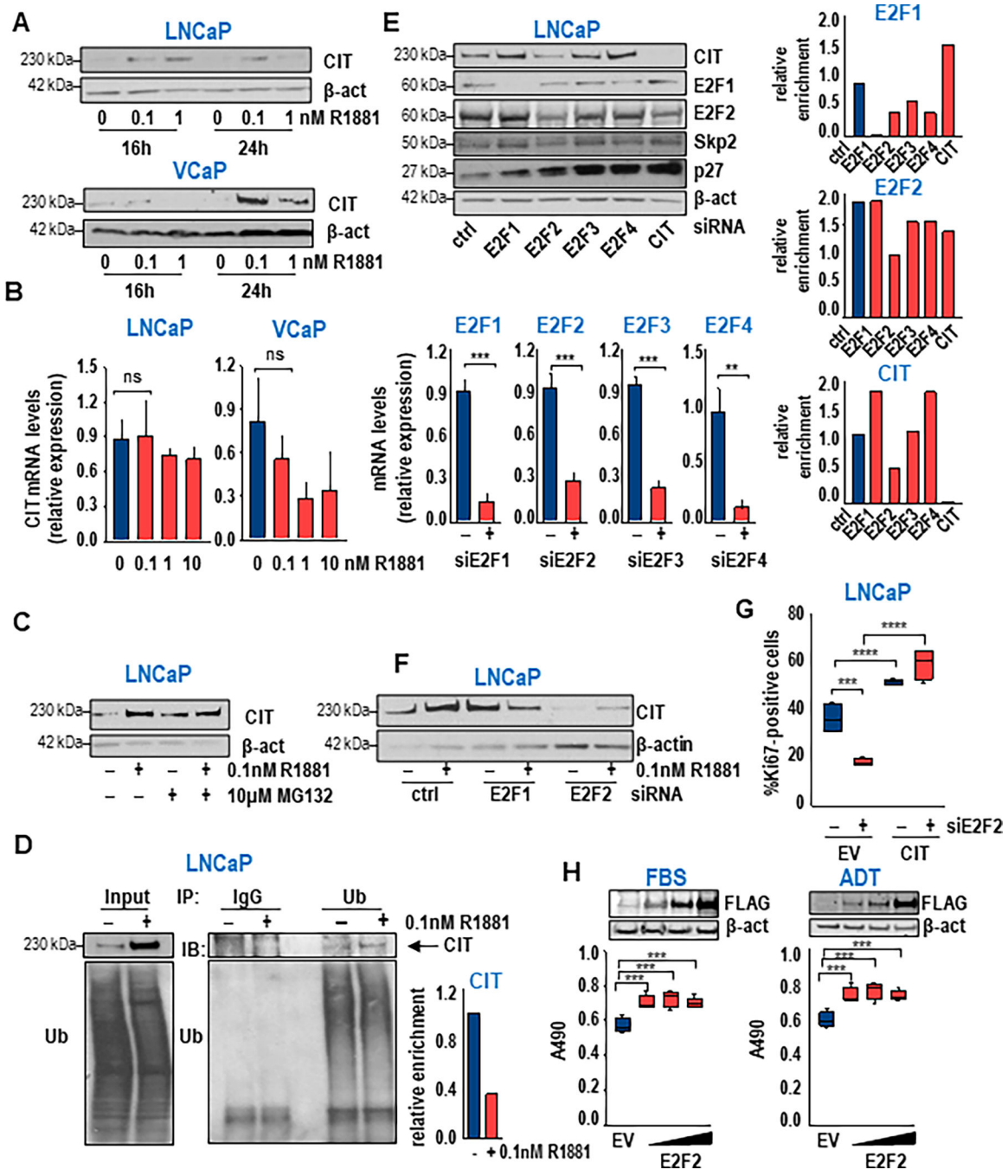


**Figure 4. Novel E2F2-Skp2-p27 pathway regulates CIT expression.**

**(A)** Time course with increasing doses of R1881 for 16h and 24h in LNCaP and VCaP cells. CIT and β-actin protein expression was analyzed via western blotting. (**B**) CIT mRNA levels determined by qRT-PCR after 24h treatment with increasing doses of R1881 in LNCaP (left) and VCaP (right). CIT mRNA levels were normalized to GAPDH expression and are represented as relative expression using the value obtained from one of the biological triplicates from the vehicle-treated condition as 1. *Columns,* means of values obtained from independent biological triplicates; *bars,* SEM. (**C**) Western blot of LNCaP cells

treated with 0.1nM R1881 or vehicle for 24h, followed by MG132 or DMSO treatment for 16h. (**D**) IP using ubiquitin-targeting antibody (ub), followed by western blotting for CIT on LNCaP cells treated with 0.1nM R1881 or ethanol for 24h. IP, immunoprecipitation, IB, immunoblotting. Arrow indicates CIT immunoreactive signal. Insert: Quantification of immunoreactive signals for IP'ed samples. Signals for IP'ed samples were normalized against the value of the matching input sample. (**E**) Western blot analysis of CIT, E2F1, E2F2, Skp2, p27 and β-actin in LNCaP cells transfected for 96h with siRNA targeting either E2F1, E2F2, E2F3, E2F4, or CIT or with non-specific control (ctrl) siRNA (top left). Quantification of E2F1, E2F2 and CIT immunoreactive signals, normalized against the value of the β-actin signal (right). E2F1, E2F2, E2F3 and E2F4 mRNA levels were determined by qRT-PCR at 96h after transfection with specific siRNAs as under B (bottom left). (**F**) Protein levels of CIT and β-actin in LNCaP cells transfected as under G with siRNA against either E2F1, E2F2 or control siRNA. Two days later cells were treated with 0.1nM R1881 or vehicle (ethanol). (**G**) LNCaP cells were transfected with siRNA targeting E2F2 or with non-specific control siRNA. At 48h after transfection, cells were transfected with expression constructs encoding wild-type CIT (CIT) or empty vector (EV). Cell proliferation was evaluated by Ki67 immunostaining. The percentage of Ki67-positive cells was recorded. si, siRNA (**H**) LNCaP cells were transfected with increasing amounts of an expression construct encoding FLAG-tagged E2F2 or empty vector (EV). Four days later, a cell viability assay reading at 490nM (in quintuplicate) was performed. Left: cells cultured in regular FBS-containing growth medium, right: cells cultured in androgen-deprived medium. **p<0.01, ***p<0.001, ****p<0.001, ns, non-significant, t-test. Box plot reflects mean ±SEM. β-act, β-actin.

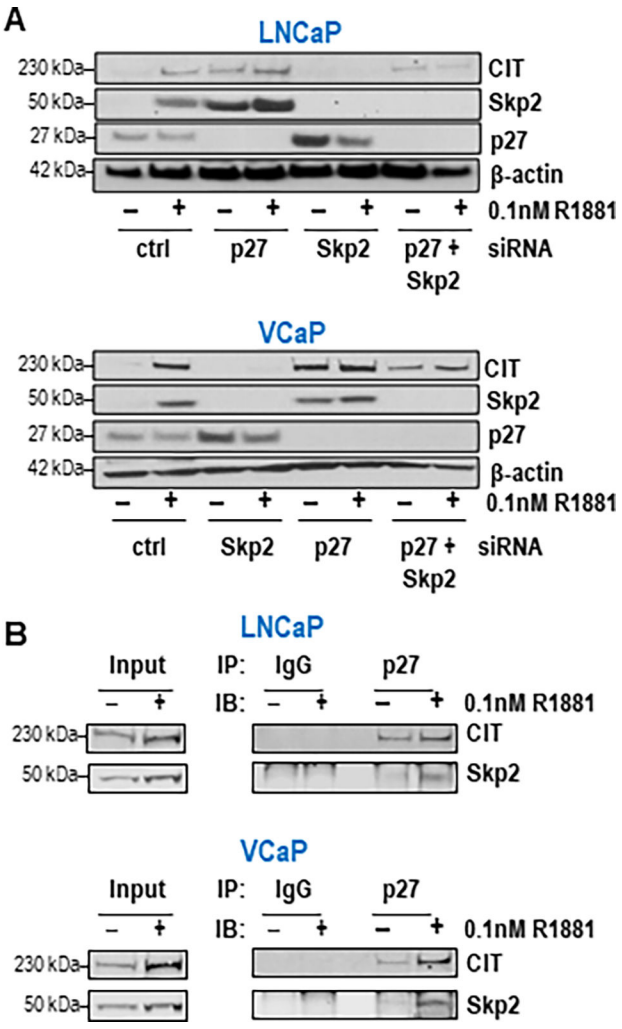


**Figure 5. E2F2 signaling leads to p27-CIT interaction**

(**A**) Western blot analysis of CIT, Skp2, p27, and β-actin levels in LNCaP (top) and VCaP (bottom) cells transfected with control siRNA or siRNA against p27, Skp2 alone or co-transfected with siRNAs targeting p27 and Skp2. Two days later, cells were treated with 0.1nM R1881 or vehicle (ethanol). Note difference in sample loading order between LNCaP and VCaP samples. (**B**) Co-IP using an antibody targeting p27 and western blotting of CIT in LNCaP (top) and VCaP (bottom) cells treated for 48h with 0.1nM R1881 or vehicle. Blot was reprobed for Skp2 as a positive control for p27 immunoprecipitation.

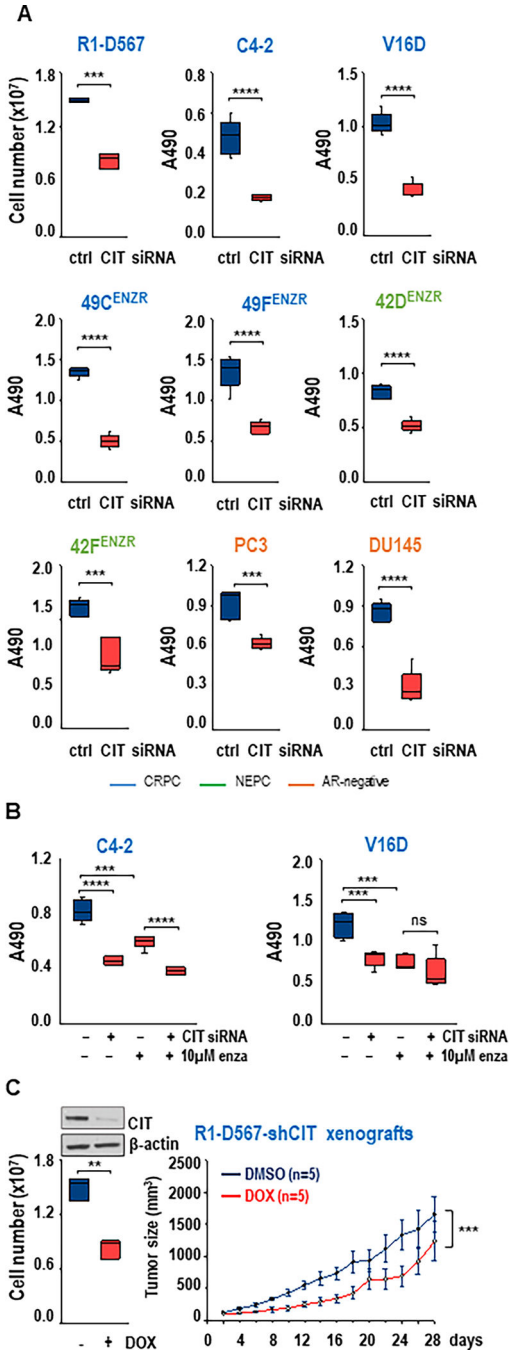


**Figure 6. CIT controls growth of CRPC, NEPC and AR-negative CaP.**

(**A**) CRPC cell lines C4–2, R1-D567, V16D, 49C$^{ENZR}$ and 49F$^{ENZR}$, NEPC cell lines 42D$^{ENZR}$ and 42F$^{ENZR}$, and AR-negative cell lines PC3 and DU145 were transfected with siRNA targeting CIT or non-targeting control siRNA (Ctrl). At 96h after transfection, cell viability was measured via trypan blue staining (R1-D567, biological triplicates) or using an MTS assay in quintuplicate (all other cell lines) read at 490nm. (**B**) LNCaP cells were transfected using siRNA targeting CIT (+) or non-targeting control siRNA (−). Two days later, cells were treated for 48h with 10μM enzalutamide (enza) (+) or vehicle (DMSO,-).

Cell viability was measured using an MTS assay read at 490nm (in quintuplicate). (**C**) Left: R1-D567 CRPC cells that express doxycycline-inducible shRNA targeting CIT#3 were treated with 1 mg/ml doxycycline (DOX) or vehicle (DMSO). At 96h after transfection, CaP cell viability was evaluated as above (bottom). CIT and β-actin expression were evaluated via western blotting (top). Right: same cell line was used in xenograft experiments. Once xenografts reached $100mm^3$, animals were randomized and treated with doxycycline (DOX, 200μg/ml in drinking water, n=5 (red) or vehicle (DMSO, n=5, blue). Tumor volumes were measured every other day for 28 days. Data are shown as mean ±SEM. A, B, C (left): **p<0.01, ***p<0.001, ****p<0.0001, t-test. C (right): ***p<0.001, 2-way ANOVA. ns, not significant.

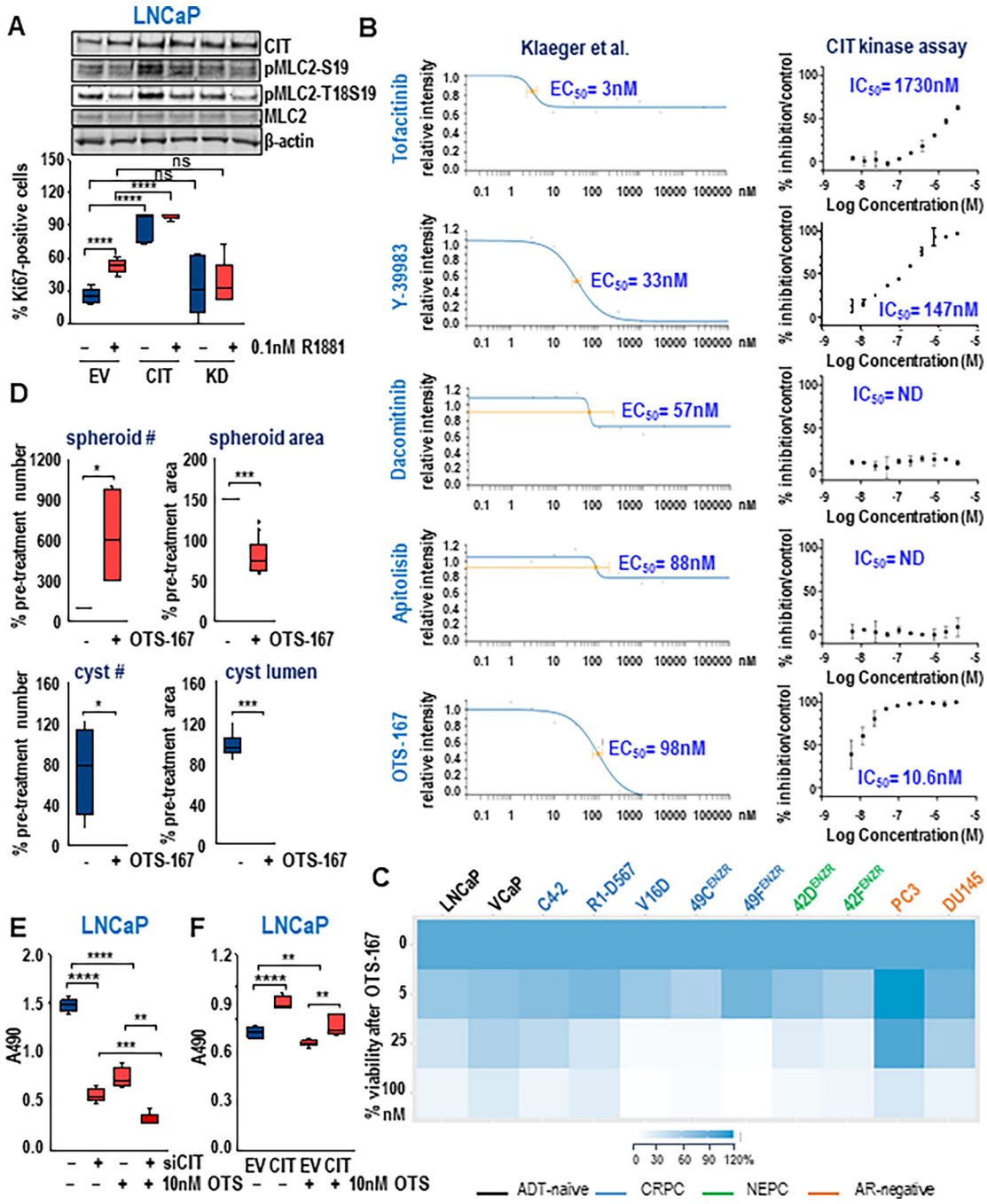


**Figure 7. CIT is a druggable target for CaP treatment.**

**(A)** LNCaP were transiently transfected with expression constructs encoding wild-type CIT (CIT), citron kinase-dead (CIT-KD), or empty vector (EV) and stimulated with 0.1nM R1881 for 48h. Ki67 immunostaining was performed and percentage of Ki67-positive cells was recorded (bottom). Western blot analysis on parallel samples verified CIT, pMLC2-S19, pMLC2-T18S19, MLC2 and β-actin levels (top) (**B**) Clinically evaluated kinase inhibitors with CIT $EC_{50}$<100nM, based on data by Klaeger et al. (43) (left). Validation of CIT inhibition by tofacitinib, Y-39983, dacomitinib, apitolisib, or OTS-167 via in vitro kinase

assays (Eurofins) (right). (**C**) LNCaP, VCaP, C4–2, R1-D567, V16D, 49C$^{ENZR}$, 49F$^{ENZR}$, 42D$^{ENZR}$, 42F$^{ENZR}$, PC3 and DU145 cells were treated with 0, 5, 25 or 100nM OTS-167 or vehicle for 4 days. Cell viability was assessed as detailed in Supplementary Figure 6, which also provides the specific assay data used to generate the heatmap shown here. (**D**) PDOs derived from the PCSD1 PDX were established. After 2 weeks, PDOs were treated with 50nM OTS-167 or vehicle (DMSO) for 72h. Spheroids and cysts were counted, measured, and values obtained after treatment were normalized using their paired pre-treatment values. (**E**) LNCaP cells were transfected using siRNA targeting CIT (+) or non-targeting control siRNA (−). Two days later, cells were treated for 48h with 10nM OTS-167 (+) or vehicle (DMSO,-). Cell viability was measured using an MTS assay read at 490nm (in quintuplicate). (**F**) LNCaP cells were transiently transfected with CIT or EV. The next day, cells were treated with 10nM OTS-167. Four days later, cell viability was measured using an MTS assay read at 490nm (in quintuplicate). Box plots reflect mean ±SEM. *, $p<0.05$, **, $p<0.01$, ***$p<0.001$, ****$p<0.0001$, t-test.

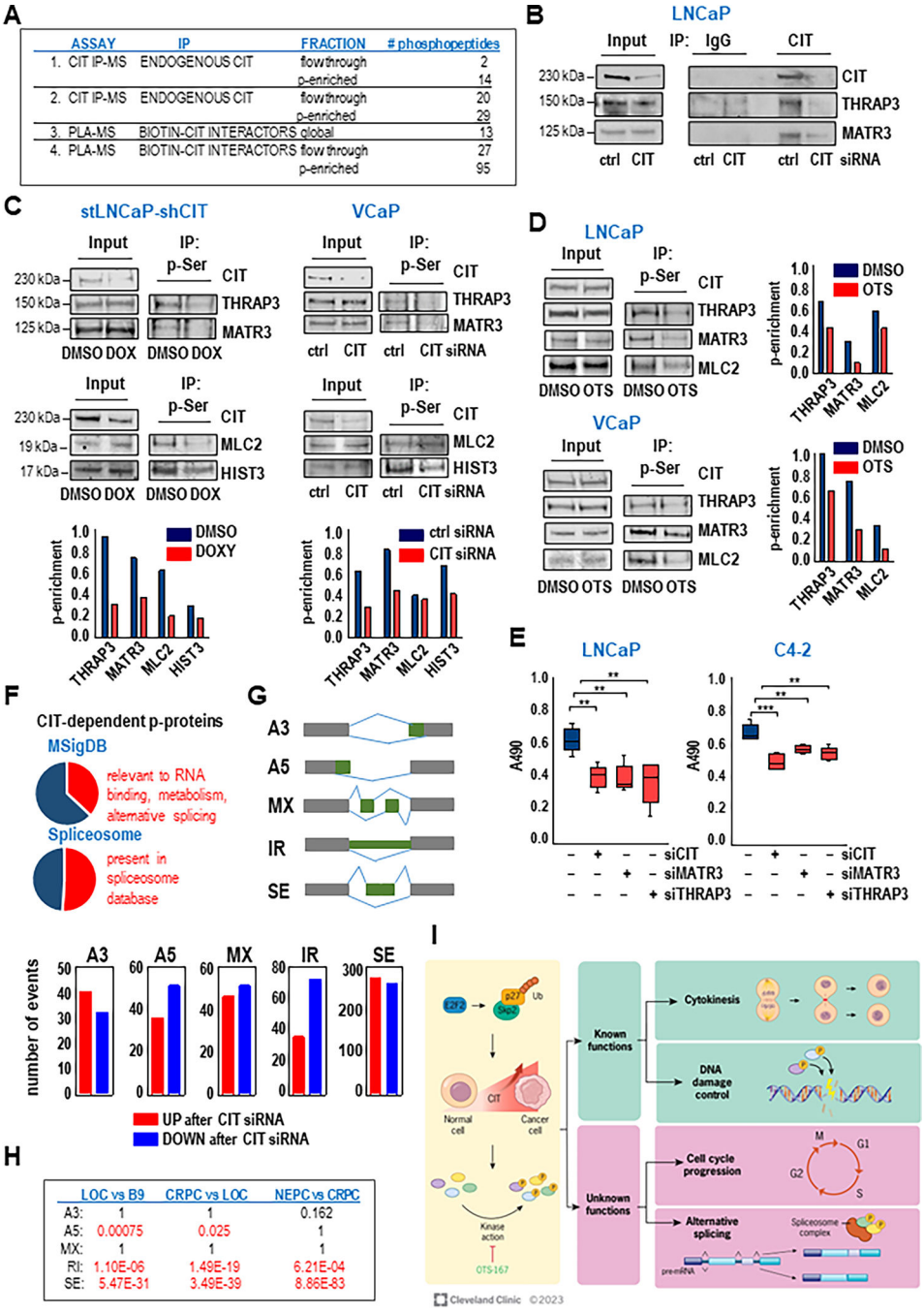


**Figure 8. Isolation of in vivo CIT substrates in CaP cells.**

(**A**) MS experiments that were performed to isolate CIT-dependent phosphomarks. IP, immunoprecipitation; MS, mass spectrometry; PLA, biotin-based proximity ligation assay using TurboID gene fusions; biotin; biotinylated proteins that interact with wild-type CIT; p-enriched, phospho-enriched. (**B**) Western blot analysis for MATR3, THRAP3, and CIT following IP with non-targeting IgG or antibody against CIT in LNCaP cells that were transfected for 96h with control siRNA or siRNAS targeting CIT. (**C**) Western blot analysis for MATR3, THRAP3, MLC2, histone 3 (HIST3) and CIT following IP with a pSer-specific

antibody. Lysates from LNCaP cells that allow for doxycycline-inducible CIT shRNA expression were used at 96h after vehicle (DMSO) or doxycyline treatment (DOX) (left). Lysates from VCaP cells were used at 96h after transfection with control siRNA or CIT targeting siRNA (right). Bottom: Quantification of immunoreactive signals for p-Ser IP'ed samples. Signals for IP'ed samples were normalized against the value of the matching input sample. (**D**) Western blot analysis for MATR3, THRAP3, MLC2 and CIT following IP with a pSer-specific antibody. Lysates from LNCaP or VCaP cells treated for 96h with DMSO or 10nM OTS-167 (OTS) were used. Right: Quantification of immunoreactive signals for p-Ser IP'ed samples as under C. (**E**) LNCaP and C4–2 cells were transfected with siRNA targeting CIT, THRAP3 or MATR3, or with non-targeting control siRNA. At 96h after transfection, cell viability was measured using an MTS assay in quintuplicate read at 490nm. Box plots reflect mean ±SEM. **p<0.01, ***p<0.001, t-test. si:siRNA. (**F**) MSigDB and Spliceosome database analyses of proteins that show CIT-dependent phosphomarks. (**G**) Overview of alternative splicing patterns. A3, alternative 3' splice sites; A5, alternative 5' splice sites; MX, mutually exclusive exons; IR, intron retention; SE, exon skipping (top panel). RNA-Seq data was analyzed for CIT-dependent splicing events using rMATS. Number and type of basal CIT-dependent splicing events (bottom panel) are shown. Red, upregulated; blue, downregulated after CIT silencing. (**H**) Enrichment of basal CIT-dependent splicing events in splicing patterns in treatment-naïve localized CaP (LOC) versus benign prostate tissue (B9), CRPC versus LOC and NEPC versus CRPC. P values shown in red are <0.05 and considered significant. (**I**) Novel insights in CIT action in CaP. E2F2-Skp2-p27-dependent mechanism in control of CIT expression in CaP and the critical role for CIT's kinase action in CaP (left). Cellular signaling and processes in which CIT-dependent phospho-proteins function include previously reported (known) functions such as those in cytokinesis and DNA damage control and novel (unknown) function suggested by the current study such as those in cell cycle progression and alternative splicing (right).